https://doi.org/10.5194/acp-2022-237
Preprint. Discussion started: 22 April 2022
© Author(s) 2022. CC BY 4.0 License.

Atmospheric Chemistry and Physics Discussions

Hydrochloric acid emission dominates inorganic aerosol formation from ammonia in the Indo-Gangetic Plain during winter

Pooja V. Pawar[1,6], Sachin D. Ghude[1], Gaurav Govardhan[1], Prodip Acharja[1], Rachana Kulkarni[2], Rajesh Kumar[3], Baerbel Sinha[4], Vinayak Sinha[4], Chinmay Jena[5], Preeti Gunwani[1], Tapan Kumar Adhya[6], Eiko Nemitz[7], and Mark A. Sutton[7]

[1]Indian Institute of Tropical Meteorology (IITM), Ministry of Earth Sciences, Pune, India
[2]Savitribai Phule Pune University, Pune, India
[3]National Center for Atmospheric Research (NCAR), Boulder, CO, USA
[4]Department of Earth and Environmental Sciences, Indian Institute of Science Education and Research Mohali, Punjab, India
[5]India Meteorological Department (IMD), Ministry of Earth Sciences, Lodhi Road, New Delhi, India
[6]Kalinga Institute of Industrial Technology (KIIT), Bhubaneshwar, India
[7]UK Centre for Ecology & Hydrology (UKCEH), Edinburgh, UK

Correspondence to: Sachin D. Ghude (sachinghude@tropmet.res.in)

Abstract. The Winter Fog Experiment (WiFEX) was an intensive field campaign conducted at Indira Gandhi International Airport (IGIA) Delhi, India, in the Indo-Gangetic Plain during the winter of 2017-2018. Here, we report the first comparison in South Asia of the high temporal resolution measurements of ammonia (NH_3) along with water-soluble inorganic ions in $PM_{2.5}$ (Cl^-, NO_3^-, SO_4^{2-} and NH_4^+) and corresponding precursor gases (HCl, SO_2, HONO, and HNO_3) made at the WiFEX research site, using the Monitor for AeRosols and Gases in Ambient Air (MARGA) and high-resolution simulations with Weather Research and Forecasting model coupled with chemistry (WRF-Chem). The hourly measurements were used to investigate how well the model captures the temporal variation of gaseous and particulate water-soluble species and gas-to-particle partitioning of NH_3, using the Model for Simulating Aerosol Interactions and Chemistry (MOSAIC) aerosol scheme. The model frequently simulated higher NH_3 and lower NH_4^+ concentrations than the observations, while total NH_x values/variability agreed well with the observations. Under the winter conditions of Delhi, high concentrations of hydrochloric acid (HCl) in the ambient air are found to dominate the gas-to-particle partitioning, as NH_3 is usually in excess. The default model set-up of WRF-Chem excludes anthropogenic HCl emissions, so sulfuric acid (H_2SO_4) dominates the gas-to-particle partitioning with NH_3 during the simulation period. The sensitivity experiments, including HCl emissions in the model, showed that the inclusion of HCl emissions improves the simulated gas-to-particle conversion rate of ammonia by 24 % (as indicated by NH_4^+ concentrations) while reducing the bias in gas phase NH_3 by 10 %. Nevertheless, even with waste burning HCl emissions included, we find that WRF-Chem still overestimates sulfur dioxide (SO_2) and nitrate (NO_3^-) formation and underestimates sulfate (SO_4^{2-}), nitrous acid (HONO), nitric acid (HNO_3), and HCl concentration in which it interacts, thus limit the gas-to-particle conversion of NH_3 to NH_4^+ in the model. This indicates that modeling of ammonia requires a correct chemistry mechanism with accurate emission inventories for the industrial HCl emissions.

https://doi.org/10.5194/acp-2022-237
Preprint. Discussion started: 22 April 2022
© Author(s) 2022. CC BY 4.0 License.

Atmospheric Chemistry and Physics Discussions

1 Introduction

The Indo-Gangetic Plain (IGP) has been one of the global hotspots of atmospheric ammonia (NH_3) and faces a range of environmental challenges, particularly during the winter season, including adverse air pollution episodes, as NH_3 plays a substantial role in secondary aerosol formation (Ghude et al., 2020, 2008b, 2008a; Kumar et al., 2021; Saraswati et al., 2019; Sharma et al., 2020; Singh et al., 2021). Atmospheric NH_3 along with oxides of nitrogen (NO_x) together account for the largest source of reactive nitrogen (N_r), which is primarily emitted by agricultural activities, livestock population, industrial activities, and transportation (Ghude et al., 2009, 2010, 2012, 2013; Móring et al., 2021; Pawar et al., 2021; Sutton et al., 2017b). NH_3 in the environment plays a crucial role in atmospheric chemistry and the eutrophication and acidification of ecosystems (Datta et al., 2012; Mandal et al., 2013; Pawar et al., 2021; Sharma et al., 2008, 2012, 2014b). Control of ammonia becomes a key priority in an emerging international strategy to manage the global nitrogen cycle (Gu et al., 2021; Sutton et al., 2020). Ammonia is a significant precursor of an aerodynamic diameter smaller than 2.5 μm ($PM_{2.5}$) containing ammonium sulfate, ammonium nitrate, and in some environments, ammonium chloride (Seinfeld and Pandis, 2016). In addition, as the dominant alkaline gas in the atmosphere, NH_3 has attracted the interest of scientific researchers since it has been known to promote new aerosol formation both in the initial homogeneous nucleation and in the subsequent growth, especially during wintertime (Acharja et al., 2020, 2021; Ali et al., 2019; Duan et al., 2021; Wagh et al., 2021).

In this study, we focus on wintertime analyses since this season is characterized by low-to-dense fog events, lower temperature (T), and variability of relative humidity (RH), which fluctuates from 40 to 100 % (Ghude et al., 2017; Kumar et al., 2020). Ammonia acts as a neutralization agent for determining the acidity of aerosol particles (Acharja et al., 2020; Ali et al., 2019; Ghude et al., 2017). It also affects the $PM_{2.5}$, acidity of clouds, and wet deposition of nitrogen by neutralizing acidic species (Gu et al., 2021; Xu et al., 2020). Increasing NH_3 concentration over Delhi compared with the surrounding area leads to an increase in $PM_{2.5}$ concentrations (Sharma et al., 2008, 2012, 2014a), which in turn affects air quality, human health, and climate (Behera et al., 2013; Ghude, 2016; Ghude et al., 2008b; Nivdange et al., 2022; Sutton et al., 2017a; Sutton and Howard, 2018).

Satellite observations (Van Damme et al., 2018; Warner et al., 2017), chemical transport models (Clarisse et al., 2009, 2010; Wang et al., 2020b), and ground-based observations (Pawar et al., 2021) revealed that the IGP is the largest regional hotspot of NH_3 concentrations on the Earth. Previous studies have identified various sources of NH_3 such as agricultural activities, industrial sectors, motor vehicles, garbage, sewage, and urine from rural populations, etc. at the global scale (Behera et al., 2013; Huang et al., 2012; Sutton et al., 2008). However, in Delhi, agricultural activity (including surrounding arable and sub-urban livestock farming) is the dominant source of NH_3, along with the traffic emissions(Kuttippurath et al., 2020; Móring et al., 2021; Sharma et al., 2020) and its emissions are subject to large uncertainty. Globally, various modeling efforts have investigated the relative effectiveness of reducing NH_3 emissions in curtailing $PM_{2.5}$ formation (Gu et al., 2021; Pinder et al., 2007, 2008; Zhang et al., 2020). However, over India, the impact on reducing $PM_{2.5}$ might be limited because NH_3 emission reductions may be more challenging due to its alkaline nature and area-wide sources. Ianniello et al. (2010) and Lan et al. (2021) have investigated the variation of atmospheric ammonia at an urban and suburban site of Beijing with respect to meteorological factors, where RH was found to be a strong factor for influencing the NH_3 mixing ratio. A few studies over Asia have highlighted the gas-to-particle

https://doi.org/10.5194/acp-2022-237
Preprint. Discussion started: 22 April 2022
© Author(s) 2022. CC BY 4.0 License.

Atmospheric Chemistry and Physics Discussions

conversion of NH_3 in Delhi (Acharja et al., 2021; Saraswati et al., 2019) and China and its subsequent impact on aerosol formation (Wang et al., 2015; Xu et al., 2020). Furthermore, excess ammonia during fog can also enhance secondary aerosol formation in Delhi during winter (Acharja et al., 2021). However, the wintertime behavior of ammonia in Delhi in chemical transport models (CTM) has not yet been investigated and remains poorly understood (Ellis et al., 2011; Metzger et al., 2006). In a recent study, Pawar et al. (2021) has highlighted uncertainties associated with gas-to-particle partitioning of NH_3 in a global model MOZART-4 and found a significant overestimation of NH_3 in the model compared with the measurements. The overestimation of ammonia in the model led the authors to hypothesize that a source-specific ammonia emission inventory in India considering agricultural statistics on the fertilizer use and animal distribution was missing. Also, there was a need for a high-resolution regional model with advanced chemistry to resolve the NH_3 emissions on the local scale.

The present study utilizes measurements from the Winter fog Experiment (WiFEX), including NH_3, water-soluble ions in $PM_{2.5}$, other trace gases, and meteorological parameters, interpreted using the regional Weather Research and Forecasting model coupled with chemistry (WRF-Chem) during December-January 2017-18. For the first time in India, we discuss and compare the observed and modeled temporal variation in NH_3, NH_4^+, and total ammonia (NH_x). Since we found that modeled NH_x matches well with the observations, we investigate the measurements and modeling associated with the gas-phase NH_3 and particulate NH_4^+ in terms of gas-to-particle partitioning. We carried out several sensitivity experiments with and without the addition of anthropogenic waste burning emissions of hydrochloric acid (HCl) in the model. The updated model with HCl emissions was used to analyze and compare the temporal variation of NH_3, NH_4^+, and NH_x from the WiFEX measurements.

2. Data and methodology

2.1 Observational datasets

In this study, we used Monitor for AeRosols and Gases in Ambient Air-model 2S (MARGA), having two channels, one for sampling PM_1 and the other channel sampling $PM_{2.5}$ for the ground-based observations. The air was first passed through two dedicated separate impactors (cut-off diameters 1 and 2.5 µm respectively) with the exit air (as PM_1 and $PM_{2.5}$) then sent through 1 cm long diameter PolyTetraFluoroEthylene (PTFE) tubes to the MARGA to achieve the separation of PM_1 and $PM_{2.5}$. The flow rate in each sampling box is regulated to a volumetric flow of 1 m^3 h^{-1}. Anions are separated in a Metrosep A Supp 10 (75/4.0) column, whereas for cations separation, a Metrosep C4 (100/4.0) cation column is used (Acharja et al., 2020). The MARGA was located inside the Indira Gandhi International Airport (IGIA), New Delhi (28.56° N, 77.09° E), with 1 cm long inlet lines sampling outdoor air at 8 m above ground and 2 m above the rooftop. Measurements covered a winter period (19th December 2017 to 21st January 2018) with frequent moderate to dense fog events. Details of the MARGA instrument can be found in Makkonen et al. (2012), Thomas et al.(2009) and Twigg et al. (2015).

Surface measurements of ambient ammonia were made along with other trace gases (HCl, HONO, HNO_3, and SO_2) and water-soluble inorganic components (Cl^-, NO_3^-, SO_4^{2-}, NH_4^+, Na^+, K^+, Mg^{2+}, Ca^{2+}) of PM_1 and $PM_{2.5}$ at an hourly resolution. In this study, we have focussed on only $PM_{2.5}$ inorganic water-soluble

https://doi.org/10.5194/acp-2022-237
Preprint. Discussion started: 22 April 2022
© Author(s) 2022. CC BY 4.0 License.

Atmospheric Chemistry and Physics Discussions

components for consistency with the selected WRF-Chem aerosol size distribution. The collected samples were analyzed in the analyzer box using the ion-chromatography (IC) technique to analyze the chemical species. For detailed information on the measurement site and its meteorological parameters, refer to (Ali et al., 2019). All the precautionary measures were taken to minimize the manual errors in preparing the internal standard solution, absorbing solution and regenerant, anion, and cation eluents to ensure the quality control of the data obtained from MARGA. The $PM_{2.5}$ impactors were typically cleaned fortnightly to remove any material that may stick on the surface and inlets of the impactors. The quality of the data obtained was then checked using the ion-balance method. Further detail on the quality control of MARGA can be found in Acharja et al. (2020).

Hourly NO_x measurements were made by the chemiluminescence method, and hourly ozone (O_3) measurements were made by the UV photometric method (CPCB, 2011) at the nearest air quality monitoring station (AQMS) of IGIA operated by the Central Pollution Control Board (CPCB). NO_x analyzers contain a thermal converter that catalytically reduces NO_2 to NO. The original NO and the NO (converted from NO_2) in the sample are then reacted with ozone (O_3) to give a total NO + NO_2 (NO_x) reading. At the same time, an ozone photometric analyzer measures O_3. These air quality monitoring stations' quality control and assurance processes were followed as outlined in CPCB (2014, 2020). For data quality, we rejected all those observed values which fell below the lowest detection limit of the instrument (1 µg m^{-3} for NO_x and 4 µg m^{-3} for O_3) (Technical specifications for CAAQM station, 2019) and above 500 µg m^{-3} for NO_x and 140 µg m^{-3} for O_3 at a given site. This step aims to remove any short-term local influence that cannot be captured in the models and retain the regional-scale variability because the nearest sites are located in the urban environment. We removed single spike represented by a change of more than 100 µg m^{-3} in just 1 hour (h) for all the data in CPCB monitoring stations to filter out random fluctuations in the observations. We removed some very high NO_x and O_3 values that appeared in the time series right after the missing values. Meteorological parameters, including air temperature (T), relative humidity (RH), wind speed and wind direction were measured with the automatic weather station (AWS) platform on a 20 m flux tower tower (Ghude et al., 2017).

2.2 WRF-Chem v 3.9.1 model

The Weather Research and Forecasting model coupled with chemistry (WRF-Chem v3.9.1) has been employed in this study to simulate atmospheric gases and aerosols over Delhi during the peak winter period, starting from 19 December 2017 to 21 January 2018. We recently used a similar model configuration to simulate the air quality over Delhi (Ghude et al., 2020; Kulkarni et al., 2020). This study used the MOZART-4 gas-phase chemical mechanism coupled with the Model for Simulating Aerosol Interactions and Chemistry (MOSAIC) aerosol scheme, including sulfate, ammonium, nitrate, methanesulfonate, sodium, calcium, chloride, carbonate, black carbon, primary and organic mass. Other inert minerals, trace elements, and inorganic species are lumped together as different inorganic masses. MOSAIC allows gas-to-particle formation, which includes NH_3, HCl, sulfuric acid (H_2SO_4), nitric acid (HNO_3), and methane sulfonic acid (MSA), and also includes secondary organic aerosols (SOA). Aerosol size distributions are represented by a sectional aerosol bin approach with four size bins (Georgiou et al., 2018). MOSAIC includes a thermodynamic module named 'Multicomponent Taylor Expansion Method' (MTEM), which is used for the calculation of the activity coefficients in aqueous atmospheric aerosols, and the 'Multicomponent Equilibrium Solver for Aerosols' (MESA), which provides a computationally efficient solution of the intraparticle solid-liquid phase equilibrium. This combined

https://doi.org/10.5194/acp-2022-237
Preprint. Discussion started: 22 April 2022
© Author(s) 2022. CC BY 4.0 License.

Atmospheric Chemistry and Physics Discussions

thermodynamic module MESA-MTEM is coupled with the new gas-to-particle partitioning module named 'Adaptive Step Time-split Euler Method' (ASTEM), which dynamically integrates the mass transfer equations. The ASTEM algorithm produces smooth, accurate and computational efficient solutions by solving the dynamic gas-to-particle conversion at low, moderate and high RHs when aerosol particles may be entirely mixed or solid phase. A new concept of "dynamic pH" along with an adaptive time stepping scheme in ASTEM algorithm reduces the stiffness in the Ordinary Differential Equations (ODEs) and produces the explicit solutions over the entire RH range. However, secondary organic aerosol (SOA) formation and their interactions with former inorganic aerosol species, primary organics, water, and particle pH are not included in MOSAIC. Moreover, their impact on gas-to-particle partitioning is poorly understood and remains an area of enormous uncertainty in chemical transport models. For further details on the MOSAIC scheme, please refer to Zaveri et al. (2008).

The model domain covers the entire northern region of India, but here model simulations are compared with the observations at IGIA, New Delhi (28.56° N, 77.09° E). The domain was set with a horizontal grid-spacing of 10 km in both the latitudinal and longitudinal directions. The model top included 47 vertical levels and was set to 10 hPa. The physical parameterization schemes of model configuration are the same as described in Ghude et al. (2020) and Jena et al. (2021). EDGAR-HTAP (Emission Database for Global Atmospheric Research for Hemispheric Transport of Air Pollution) for the year 2010 at 0.1º x 0.1º grid resolution has been used in this study for anthropogenic emissions of aerosols and trace gases ($PM_{2.5}$, PM_{10}, OC, BC, CO, NO_x, etc.) and are scaled to 2018 as per Jena et al. (2021). Biogenic emissions are calculated online using the Model of Emissions of Gases and Aerosols from Nature version 2.1 (MEGAN2.1) (Guenther et al., 2006), and dust emissions are based on online Atmospheric and Environmental Research Inc. and Air Force Weather Agency (AER/AFWA) scheme (Ginoux et al., 2001). Fire INventory from NCAR (FINNv1.5) has been used in this study for daily open biomass burning emissions. The chemical initial and lateral boundary conditions come from the global model simulations from the Model for Ozone and Related Chemical Tracers (MOZART-4), and the meteorological initial and lateral boundary conditions are provided from the fifth generation European Centre for Medium-Range Weather Forecasts (ECMWF) atmospheric reanalysis of the global climate (ERA5) with six-hourly temporal resolution. The simulations were reinitialized every fifth day to limit the growth of meteorological errors in our simulations, but the chemical fields were carried forward from the previous simulation.

3. Results and Discussion

3.1 MARGA

3.1.1 Temporal variation in NH_3 and NH_4^+

Figure 1 displays the diurnal variation (00:00 to 23:00 Indian Standard Time (IST)) in NH_3 and NH_4^+ averaged over all the study period (Fig. 1a) along with meteorological parameters (temperature and RH) at the IGIA site in Delhi (Fig. 1b). As indicated in Fig. 1a, the average NH_3 concentration maxima and minima were observed during 08:00-12:00 h and 01:00-07:00 h, respectively. The mean ± 1σ, median, maximum and minimum values in the average diurnal NH_3 concentration for the observation period were 28.20 ± 12.37, 28.45, 40.98, and 20.09 µg m^{-3} respectively. The NH_3 concentration gradually increased during 17:00-1:00, decreased from 1:00-7:00 h,

https://doi.org/10.5194/acp-2022-237
Preprint. Discussion started: 22 April 2022
© Author(s) 2022. CC BY 4.0 License.

Atmospheric Chemistry and Physics Discussions

and then rapidly increased from 08:00 h (just after sunrise). After reaching the peak at approximately 12:00 h, a decrease was observed until it came to the minimum of 25.65 μg m^{-3} at 15:00 h. The mean ± 1σ, median, maximum and minimum values of the average diurnal NH_4^+ concentration during the study period were 36.96 ± 15.10, 39.25, 46.28, and 21.45 μg m^{-3} respectively. While the average NH_4^+ concentration maxima and minima were observed during night time (16:00-03:00 h) and daytime (03:00-08:00 and 09:00-16:00 h), respectively. The daytime increase in NH_3 concentration could be associated with NH_4^+ aerosol volatilization driven by associated increases in temperature, which was observed mainly from 08:00 h onwards. This indicates that an increase in NH_3 concentration in the morning is caused by meteorological conditions. From Fig. 1b, RH (T) was observed to be relatively constant before 08:00 h but decreased (increased) sharply in the later morning. High temperature and low RH contribute significantly to the evaporation of NH_3 from ammonium volatilization (Acharja et al., 2020; Sutton et al., 2009, 2013), indicating gas-to-particle partitioning impacts the diurnal behavior of ammonia at Delhi during winter. Recent studies have confirmed that evaporation of NH_3 from plants, human sources, plant stomata, morning traffic, fertilized soil, mixing down of ammonia concentration from the residual layer and dew contributes to the morning increase in NH_3 (Ellis et al., 2011; Meng et al., 2018; Norman et al., 2009; Sutton et al., 2001).

The average diurnal profile of NO_x from the nearby CPCB site (RK Puram station) is displayed in Fig. S1 in the Supplement. A similar variation for NO_x was also observed by Chate et al. (2014) and Ghude et al. (2008a) over Delhi in the previous studies. It can be seen that NO_x concentrations increase in the morning till 9:00 h, followed by a sharp decrease in the afternoon, and reach maximum concentrations in the evening around 17:00-19:00 h. Morning and evening peak coincides with the rush hour of traffic flow during the peak hour. However, it is evident that the observed morning peak of NH_3 was not concurring with corresponding NO_x peaks, suggesting that traffic emissions do not contribute significantly to the observed NH_3 rise.

During dense fog events, a significant amount of dew formation and deposition occurs on the surface is common during winter over Delhi (Ghude et al., 2017). Studies have shown that a significant amount of ammonia trapped in liquid water condensed on surfaces is released due to evaporation of dewdrops after sunrise Sutton et al. (1998). Hence, we examine how extreme dense fog and non-fog events (clear days) impact the diurnal variation of NH_3. Figure S2 in the Supplement shows the diurnal variation of NH_3 on dense fog events (13 days), which sustain more than four hours with visibility less than 200 m and on clear days with visibility more than 1000 m (20 days). Figure S2 indicates that the NH_3 morning spike phenomenon is most prevalent during the extreme dense fog events compared to clear days. The magnitude of increase in NH_3 during foggy days is two times higher with a maximum of 65 μg m^{-3} compared to the clear days with maxima 35 μg m^{-3}, indicating strong evidence that dew evaporation and the early morning NH_3 increases are linked The observed NH_3 morning peak phenomenon during foggy days suggests that dew droplets may also act as an adequate NH_3 night-time reservoir and emission sources during the day. However, we are not focussing on this aspect in the manuscript. The observed increase in morning peak (08:00 h) at IGIA could be explained by the release of NH_3 from the dew evaporation. Moreover, the contribution of dew evaporation and guttation water droplets for causing morning NH_3 peaks requires further investigation.

Since the IGIA site is surrounded by the local agricultural activities, including surrounding arable and sub-urban livestock farming should be a prime source contributing to NH_3 concentration levels (Kuttippurath et al., 2020) in addition to dew acting as a night-time reservoir of NH_3 and subsequently a morning source for

https://doi.org/10.5194/acp-2022-237
Preprint. Discussion started: 22 April 2022
© Author(s) 2022. CC BY 4.0 License.

Atmospheric Chemistry and Physics Discussions

atmospheric ammonia. Hence, in this study, analysis from the above aspects such as ammonium volatilization and dense fog events pointed to the conclusion that the ammonium volatilization and evaporation processes of dew and fog water were the cause for the morning rise of ammonia. Potential sources of NH_3 and NH_4^+ are discussed further in the next section.

3.1.2 Potential sources of NH_3 and NH_4^+

We investigated the directions of local emission sources associated with the rise in NH_3, NH_4^+ concentrations, and partitioning ratio of NH_4^+ to a total ammonia ($NH_x = NH_3 + NH_4^+$) (NH_4^+/NH_x) by the bivariate polar graphs using the OpenAir software (Carslaw and Ropkins, 2012) at the IGIA site. Figure 2 shows the wind rose (Fig. 2a) and bivariate polar plots of mean NH_3 (Fig. 2b), NH_4^+ (Fig. 2c), hydrochloric acid (HCl) (Fig. 2d), chloride (Cl^-) (Fig. 2e) concentration, and partitioning ratio of NH_4^+ to total ammonia ($NH_x = NH_3 + NH_4^+$) (NH_4^+/NH_x) (Fig. 2f) for the observation period in relation to wind speed and wind direction. The frequency of local wind indicates that the dominant direction from which air masses arrived at the IGIA site was from the 270-300º sector (Fig. 2a). The bivariate polar plot of gas-phase NH_3 in Fig. 2b shows that NH_3 emissions are highest in the east and southeast of the site, indicating a dominant source of ammonia in that direction. The IGIA site is surrounded by intense agricultural areas having various agricultural and fertilizer sources located within 200 km of Delhi and towards the east and southeast of the site (Kuttippurath et al., 2020). Additionally, large numbers of local dairy farms are also situated towards the east and southeast of the site. The discharge of wastewater and cow dung into the drains from the local dairies can contribute a major portion of agricultural ammonia emissions since 66 dairies were shut down recently by The Delhi Pollution Control Committee (DPCC) for violating environmental norms and polluting water bodies in southeast Delhi (Hindustan Times, 2021). This enhancement in the southeast region may also be related to lower wind speed, falling in the leeward side of the wind direction. Ammonia concentrations are generally higher at lower wind speeds because of turbulent diffusion (Ianniello et al., 2010).

The bivariate polar plot of NH_4^+ (Fig. 2c), HCl (Fig. 2d), and Cl^- (Fig. 2e) concentration indicates west and north-west direction as a principal source from various industries and thermal power plants which are located towards the same direction of IGIA site (Acharja et al., 2021; Kuttippurath et al., 2020; Singh et al., 2021). The ratio of NH_4^+/NH_x has been used to identify the source of NH_x and the relative contribution of NH_3 to aerosol formation. A higher ratio indicates that NH_x is primarily due to the conversion of NH_3 to salt has proceeded and thus dominates the NH_x. The polar plot of the NH_4^+/NH_x ratio in Fig. 2f identified sporadic high ratio originating from the prevailing wind direction of the IGIA site in the west direction with lower wind speed which is associated with the formation of ammonium chloride (Fig. 2c and e) from the local industrial source of HCl located north-west (NW) of the site (Acharja et al., 2021). Two sources stand out-an industrial clusters in NW Delhi, such as steel pickling industries which are known to be a vital HCl source, and metal finishing and electroplating towards the west, which impacts the site (falling in the region of high wind speed) (Fig. 2d and e) (Jaiprakash et al., 2017). Near the source, HCl is immediately available for neutralizing NH_3 (Fig. 2b and d), hence high NH_4^+/NH_x ratio towards the west (Fig. 2f) indicates that NH_3 neutralization by HCl is more critical, which dominates ammonium chloride formation (Fig. 2c and e) at lower wind speeds. The nearest industrial areas are located ~8–9 km Northwest of IGIA site houses industrial units related to metal product manufacture, scrap metal processing, plastic, rubber, pigment industries, etc. Emissions from these industrial processes and/or

https://doi.org/10.5194/acp-2022-237
Preprint. Discussion started: 22 April 2022
© Author(s) 2022. CC BY 4.0 License.

Atmospheric Chemistry and Physics Discussions

fuel oil combustion in these areas might be necessary at the study site. Thus, high NH_4^+/NH_x correspond to the lowest NH_3 concentration region (inverse relation), which can be observed in Fig. 2b and f and also correspond to the highest chloride concentration region (Fig. 2b and e).

3.2 Comparison of temporal variation in NH_3, NH_4^+, and NH_x using WRF-Chem and MARGA

3.2.1 Diurnal variation

To investigate how well a state-of-the-art chemical transport model performs in capturing the diurnal behavior of NH_3 and NH_4^+, we looked at the observed and model-simulated diurnal profiles of NH_3 and NH_4^+. We adopted diurnal variation in emissions from a recent study by Jena et al. (2021). We first investigated the ability of WRF-Chem to accurately predict the meteorological parameters of RH and T, which are important determinants of the gas-to-aerosol partitioning of volatile compounds. As shown in Fig. 3b and 8 (k and l), the simulated temperature and relative humidity are in reasonable agreement with the observations, with the simulated RH values falling in the range of 50–90 %.

Figure 3a shows the comparison of diurnal variations in the NH_3 and NH_4^+ concentration between MARGA measurements and model simulations for the observation period. Figure 3a shows that the model simulated NH_3 and NH_4^+ are very different compared with the MARGA observations. There is an average NH_3 and NH_4^+ mass loading of 56.75 ± 14.28 and 14.71 ± 4.90 µg m^{-3} respectively, in the model. We find the diurnal variation of gas-phase NH_3 is significantly overestimated by the model (Normalised Mean Bias (NMB) = 1.02). On the contrary, NH_4^+ is underestimated by about 60 % (NMB = -0.60). Simulated ammonia concentrations peak between 7:00-9:00 and 22:00-23:00 h with bimodal variation, though observations show a single peak around 12:00-13:00 LT. On the contrary, a nearly flat diurnal profile of NH_4^+ is predicted by the model. Figure 3b depicts that overall the model shows cold and wet bias compared to the observations but shows warm bias (about 2-3 ºC) and dry bias (about 10-12 %) in the afternoon hours. In spite of the small change of the amplitude of the diurnal cycle of RH, the phase characteristics of the diurnal cycle of both temperature and relative humidity are reasonably well captured by the model. Because the largest increase in simulated ammonia also precedes the large changes in simulated meteorological parameters, which is not the case in the model, and because the simulated particulate ammonium is flat compared to observations, simulated meteorology is ruled out as a significant contribution to high bias in simulated ammonia. It is hence necessary to understand other processes responsible for the overestimation of NH_3 and underestimation of NH_4^+ in the model.

3.2.2 Daily mean variations

Figure 4 displays the comparison of daily mean variations in the NH_3 (Fig. 4a), NH_4^+ (Fig. 4b), and NH_x (Fig. 4c) concentration between MARGA measurements and model simulations. The model shows large differences in NH_3 and NH_4^+ compared with MARGA (Fig. 4a and b). We find a consistent high positive bias in daily mean NH_3 (NMB = 1.02 with fair correlation, r = 0.54) in the model and negative bias in NH_4^+ (NMB = -0.62) with poor correlation (r = -0.08). Whereas, NH_x (Fig. 4c) shows low bias (NMB = 0.08, r = 0.60) between the model and observation. Despite the adequate ability of the model to reproduce the total amount of the measured ammonia (NH_x), the model is biased low for NH_4^+ and high for NH_3, indicating that incorrect gas-to-particle partitioning could be responsible for the large bias for NH_3 in the model. To understand if gas-to-particle

https://doi.org/10.5194/acp-2022-237
Preprint. Discussion started: 22 April 2022
© Author(s) 2022. CC BY 4.0 License.

Atmospheric Chemistry and Physics Discussions

partitioning is the main cause for the discrepancy in the model vis-a-vis the observations, comparing the ratio of gas-to-particle partitioning of ammonia in the measurements can help elucidate the contributing process.

3.3 Gas-to-particle partitioning of NH_3

Figure 5 shows the percentage contribution of gases (NH_3, SO_2, HCl, HNO_3, and HONO) and $PM_{2.5}$ aerosol (NH_4^+, SO_4^{2-}, NO_3^- and Cl^-) during WiFEX measurements. The pie charts for the gases show that a high amount of NH_3 (53.28 %) is a significant gas, followed by sulfur dioxide (SO_2) (35.61 %). Ammonia is one of the highly alkaline gases that act as a precursor for aerosol formation. In the atmosphere, NH_3 reacts rapidly with H_2SO_4, HNO_3, and HCl to form ammonium sulfates ($(NH_4)_2SO_4$, and in low NH_3 environments also NH_4HSO_4), ammonium nitrate (NH_4NO_3), and ammonium chloride (NH_4Cl), respectively. The principal reactions of NH_3 with H_2SO_4, HNO_3, and HCl in the gas-to-particle partitioning process to produce ammonium salts of $PM_{2.5}$ are summarized in reactions R1 to R3 (Seinfeld et al., 1998).

$$2NH_{3(g)} + H_2SO_{4(g)} \leftrightarrow (NH_4)_2SO_{4(s)} \quad \text{(R1)}$$

$$NH_{3(g)} + HNO_{3(g)} \leftrightarrow NH_4NO_{3(s)} \quad \text{(R2)}$$

$$NH_{3(g)} + HCl_{(g)} \leftrightarrow NH_4Cl_{(s)} \quad \text{(R3)}$$

Figure 5 shows that HCl concentration (1.09 %) is comparatively low than SO_2 (35.61 %), but HCl is immediately available for neutralizing NH_3. Hence near the sources (Fig. 2d), NH_3 neutralization by HCl (R3) is more critical than H_2SO_4 neutralization (or indeed HNO_3). Also, the formation of NH_4Cl (R3) is favored under conditions of high relative humidity and low temperature (Ianniello et al., 2011; Seinfeld and Pandis, 2016), which was the case during WiFEX. Hence, as indicated in Fig. 5, on average, the anions in $PM_{2.5}$ are almost exactly neutralized by NH_4^+ (49.54 %), with Cl^- (29.69 %) as the primary anion. But the pie chart for the gases shows a very high amount of SO_2, reaching the site from the nearby industrial area, which is not converting to SO_4^{2-} very quickly. In the atmosphere, gas-phase oxidation of SO_2 occurs either through its reaction with the hydroxyl radical (OH) or in the aqueous phase, through reaction with hydrogen peroxide (H_2O_2) or ozone (O_3) (Luhana et al., 2007). However, in an ordinary ammonia-rich atmosphere, SO_2 oxidation to SO_4^{2-} due to O_3 reaction is faster than the typical gas-phase reaction rates at high pH (pH >= 4) (Seinfeld and Pandis, 2016) and could contribute ~ 51 % to the total sulfate production (Li et al., 2020), while during fog days, the two mechanisms have been found to dominate SO_2 oxidation such as the S(IV) to S(VI) conversion catalyzed by NO_2 and HONO (Yang et al., 2019) and the S(IV) oxidation catalyzed by transition metal ions (TMI) (Harris et al., 2013) which could contribute to the rest 49 % in the sulfate production (Li et al., 2020), but their quantification over our study location needs to be carried out in the future (Wang et al., 2020a).

The primary SO_2 sources are located NW of the site (Acharja et al., 2021), which limits SO_2 oxidation to SO_4^{2-} in particular for fresh plumes originating in a nearby industrial area (Jaiprakash et al., 2017). Additionally, during this study period, average O_3 concentrations (46.78 µg m^{-3}) are also low daytime (10:00-17:00 LT) at the IGIA site (Fig. S3 in the Supplement) compared to the nearest CPCB site (86.65 µg m^{-3}); thus, SO_2 oxidation to SO_4^{2-} is limited during WiFEX.

https://doi.org/10.5194/acp-2022-237
Preprint. Discussion started: 22 April 2022
© Author(s) 2022. CC BY 4.0 License.

Atmospheric Chemistry and Physics Discussions

To gain insight into the role of NH_4^+ in the neutralization of anions (Cl^-, NO_3^- and SO_4^{2-}), aerosol neutralization ratio (ANR) was calculated using the observed data. The ANR is defined as the equivalent ratio of NH_4^+ to the sum of Cl^-, NO_3^- and SO_4^{2-} because these species represent the dominant cations and anions in $PM_{2.5}$, respectively. We consider these four significant ions since they constituted 97.3 % of the total measured ions in $PM_{2.5}$ and the remaining ionic species (i.e., Na^+, K^+, Mg^{2+}, and Ca^{2+}) contributed only about 3 % of the total measured ions (Acharja et al., 2020). Figure 6 demonstrates how well the charge balance between Cl^-, NO_3^- and SO_4^{2-} (in µeq m^{-3}) as the anions and ANR works. It can be seen that acidic components were utterly neutralized by NH_4^+ with ANR values close to unity with Cl^- as a significant anion followed by NO_3^- and SO_4^{2-}. The average ANR value for $PM_{2.5}$ during the observed period was 1.08 ± 0.16. This indicates the winter period was favoring the dominant formation of hygroscopic ammonium salts (NH_4Cl, NH_4NO_3, and $(NH_4)_2SO_4$).

The ratio of NH_4^+/NH_x is calculated to evaluate the measured and modeled conversion rate of ammonia to ammonium formation. Previous studies have reported the role of NH_3 in the NH_4^+/NH_x ratio (Pawar et al., 2021; Saraswati et al., 2019; Wang et al., 2015). Here, we compare MARGA measurements and model results at the IGIA site to investigate the conversion rate of ammonia to aerosol formation for the study period. Figure 7 shows the relationship between measured (Fig. 7a and b) and modeled (Fig. 7c and d) gas-to-particle conversion ratio (NH_4^+/NH_x) with dominant cation (NH_4^+) and anion (Cl^-) (Fig. 7a and b) and dominant cation (NH_4^+) and anion (SO_4^-) mass concentration (Fig. 7c and d). In Fig. 7a, NH_4^+/NH_x was found to be directly proportional to NH_4^+ concentration with correlation coefficient (r) = 0.79, and in Fig. 7b, compared to other aerosols (statistical indicators are summarised in Table 1 (first column)), NH_4^+/NH_x was found to be directly proportional to chloride concentration (r = 0.79) which were significant at IGIA site for the observational period (Fig. 5 and 6) (Acharja et al., 2021). This indicates high conversion rate of ammonium from gaseous to particle-phase enhanced the formation of chloride aerosol during the WiFEX. The strong correlation coefficient of ammonium and chloride concentration explains that $PM_{2.5}$ is composed predominantly of converted ammonium and chloride from the reactions of ammonia with HCl (Fig. 5). Furthermore, NH_4^+/NH_x was inversely proportional to the ambient ammonia (r = -0.57) and nitrous acid (HONO) (r = -0.24) concentrations (Table 1 (first column)), indicating atmospheric inter-conversion of NH_x between its gas and particle phases. The co-variability of NH_3 and HONO suggests that the abundance of NH_3 may enhance HONO formation, which in turn could increase secondary aerosol formation (Fu et al., 2019; Ge et al., 2019). However, in a future study understanding the role of HONO in promoting secondary aerosols via the heterogeneous reactions pathway is required.

The relationship between the NH_4^+/NH_x with all gases and aerosols is investigated to understand the role of gas-to-particle conversion of NH_3 in the model, and statistical values are summarized in Table 1 (second column). The role of ambient NH_3 in the formation of $(NH_4)_2SO_4$ is indicated by the significant positive linear relationship of NH_4^+/NH_x ratio with ammonium (r = 0.67) and sulfate (r = 0.77) in the model. Figures 7c and d show the relationship between modeled NH_4^+/NH_x ratio with ammonium and sulfate concentration. The high conversion rate of ammonium from gaseous to particle-phase indicates the formation of sulfate, and then nitrate (r = 0.57) aerosols are enhanced in the model (Table 2 (second column)). Since the MOSAIC scheme is based on the order of increasing volatility of the associated ammonium compounds (Zaveri et al., 2008), hence H_2SO_4 (non-volatile) has a stronger affinity with NH_3, ammonia first reacts with it to form $(NH_4)_2SO_4$, then it reacts with semivolatile gases HNO_3 to form NH_4NO_3 (R1 and R3). Hence, NH_4SO_4 was more likely to form first in

https://doi.org/10.5194/acp-2022-237
Preprint. Discussion started: 22 April 2022
© Author(s) 2022. CC BY 4.0 License.

Atmospheric Chemistry and Physics Discussions

the model, as indicated by the higher correlation value of NH_4^+/NH_x with ammonium and sulfate as compared to NH_4NO_3. However, the observations at IGIA indicate that the presence of HCl concentration (Fig. 2d) enhances chloride concentration (Fig. 2e) which plays a significant role in the gas-to-aerosol partitioning of NH_3 in Delhi compared to other aerosols. Hence in order to improve the efficiency of the model in determining the gas-to-particle conversion of NH_3 and subsequently improving $PM_{2.5}$ predictions, it is necessary to add anthropogenic HCl emissions, which are currently missing in the default set-up of the model.

3.4 Sensitivity case study on the effects of addition of HCl emissions on the simulated NH_3 in WRF-Chem

We turn our attention to exploring the effects of the addition of anthropogenic HCl emissions on the simulated NH_3 concentration. Other recent studies have identified significant concentrations of aerosol Cl^- in cities across India, and evidence suggests that this primarily derives from HCl emitted from the open trash burning (Cash et al., 2021; Gani et al., 2019; Gunthe et al., 2021; Reyes-Villegas et al., 2021) and the nearby industrial sources (Jaiprakash et al., 2017). We, therefore, employ the HCl emissions from trash burning activities in Delhi as predicted by Sharma et al. (2019) in our model set-up. We have carried out a few sensitivity experiments for the period 7th to 16th January 2018 (10 days) by including the HCl emissions in the model to study their impact on the model simulations. We carried out three experiments for this purpose. In sensitivity experiment-1, we run the model with default set-up without HCl emissions. In sensitivity experiment-2, we tripled the original HCl emissions of Sharma et al. (2019) because the revised emission inventory was 2.9 times higher compared to those in the Sharma et al. 2019 emission inventory. Hence, we consider this a base case of HCl emissions, presuming the more recent upward adjustments in the amount of waste burned in landfills (Chaudhary et al., 2021). In the third experiment (sensitivity experiment-3), we tripled the base case HCl emissions to take into account missing industrial HCl sources. Figure 8 presents the box-whiskers plots for secondary inorganic aerosols and trace gases from the MARGA, and meteorological parameters from the AWS and those simulated by the model for the three different sensitivity experiments. As can be observed from Fig. 8a-c with increasing HCl emissions, NH_4^+ concentrations increase, and NH_3 gas-phase concentrations decrease, chloride concentrations increase drastically in all the three sensitivity experiments (Fig. 8f), and total NH_x concentrations increase slightly. Higher HCl concentrations promote the gas-to-particle conversion of excess NH_3, which in turn enhances ammonium and chloride concentration in the sensitivity experiment-3. This is further discussed in the next section. Increasing HCl emissions by a factor of three in the sensitivity experiment-3, the model simulatesNH_4^+ concentration (up to 70 µg m^{-3}) and Cl^- concentration (up to 110 µg m^{-3}) that compare reasonably well within the observed range, but continues to overestimate NH_3 concentration.

The simulated sulfate concentration (Fig. 8e) was underestimated mainly (~ 40 – 50 %) by the model in all the experiments compared with the observations. The gas-phase SO_2 simulated by all the three model experiments was found to be slightly overestimated by about 10 to 15 µg m^{-3}. This is caused by the fact that neither the S(IV) to S(VI) conversion catalyzed by NO_2 nor (Yang et al., 2019) the S(IV) oxidation catalyzed by TMI (Harris et al., 2013) is currently included in the MOSAIC mechanism. Wang et al. (2020) proposed a mechanism in which dissolved NO_2 oxidizes S(IV) to S(VI) and produces HONO, which can either partition into the gas phase or oxidize another molecule of S(IV) to S(VI). The latter reaction produces N_2O, which partitions into the gas phase. The inclusion of this mechanism into the MOSAIC scheme is likely to significantly improve the overestimation of NH_3, SO_2, and NO_3^- as well as the underestimation of SO_4^{2-} and HONO in the

https://doi.org/10.5194/acp-2022-237
Preprint. Discussion started: 22 April 2022
© Author(s) 2022. CC BY 4.0 License.

Atmospheric Chemistry and Physics Discussions

model. Furthermore, sulfate is produced (SO_2 oxidized to sulfuric acid H_2SO_4) via aqueous-phase oxidation of S(IV) by O_3, and a heterogeneous nucleation rate from sulfuric acid (H_2SO_4) is likely not efficiently simulated by the model since ozone concentration is low in the model compare with the observations (Fig. S4 in the Supplement). However, we also compared the cloud fraction of the model and from the Moderate Resolution Imaging Spectroradiometer (MODIS) satellite, and we found that the lower cloud fractions (Fig. S5 in the Supplement) could also lead to relatively weaker aqueous phase sulfate production and hence lower sulfate mass in the model (Bucaram and Bowman, 2021; Sha et al., 2019).

The simulated nitrate concentration (Fig. 8d) is generally higher in all the three sensitivity experiments; since the main neutralizing species for NO_3^- is NH_4^+, it is controlled via the equilibrium between nitrate, HNO_3, and NH_3. Simulated HNO_3 and HONO are significantly underestimated (~ 3-5 times) by the model compared to the observations, due to which nitrate formation is entirely ruled by gaseous NH_3 and HNO_3. Also, overestimating the NO_x concentration in the model compared with the observations (Fig. S6 in the Supplement) and incorrect gas-to-aerosol partitioning can allocate too much NO_3^- into the aerosol phase, so it might not leave enough in the gas phase. This could partly be a consequence of NH_3 being too high in the model and may somewhat lead to these positive discrepancies (Bucaram and Bowman, 2021; Sha et al., 2019). The extent to which sulfate is neutralized and NH_4NO_3 and NH_4Cl is formed are mainly governed by thermodynamic equilibrium, which is solved by MTEM-MSEA (Multicomponent Taylor Expansion Method and Multicomponent Equilibrium Solver for Aerosols) module used in MOSAIC (Zaveri et al., 2008). Hence, excess ammonia, after neutralizing H_2SO_4, consumes HNO_3 forming NH_4NO_3, which may further underestimate HNO_3 concentration.

Overall the missing heterogeneous chemistry in the formation of HNO_3 and HONO along with its gas-to-particle partitioning to ammonium nitrate, may not be efficient in the model (Archer-Nicholls et al., 2014). Hence, different treatments of the gas-to-particle partitioning from the nitric acid to ammonium nitrate as a function of humidity (Balzarini et al., 2015; Georgiou et al., 2018) could result in biases in nitrate concentration in the presence of higher NH_3 levels. In the future, an updated WRF-Chem model with the currently known sources and chemistry of HONO and HNO_3 and its parameterization is required to accurately determine the chemistry of NH_3, NO_x, and other aerosols (Zhang et al., 2017).

To investigate the further impact of sensitivity experiment-3 in the model, uptake of gaseous NH_3 to form NH_4Cl is analyzed by the correlation coefficient values of r = 0.86 between NH_4^+/NH_x with ammonium concentration and r = 0.84 between NH_4^+/NH_x with chloride concentration, indicating gas-to-particle conversion in the model correlates well with both the ammonium and chloride concentration. A higher ratio indicates that the model is able to form NH_4Cl from the conversion of NH_3 with HCl and was reasonably well simulated in the sensitivity experiment-3. It can be noted that it required three times increased base case HCl emissions to be able to form NH_4Cl in the sensitivity experiment-3.

3.5 Comparison of the temporal behavior of NH_3, NH_4^+, and NH_x of MARGA with all the sensitivity experiments of the model

We further compare the diurnal behavior of NH_3, NH_4^+, and NH_x using both the model and observations to develop and improve model accuracy in simulating complex short-lived ammonia. Figure 9 presents the diurnal variation of mean ammonia (Fig. 9a), ammonium (Fig. 9b), and total ammonia (Fig. 9c) concentration for all three different sensitivity experiments. While the simulated NH_3 concentration decreases in sensitivity

https://doi.org/10.5194/acp-2022-237
Preprint. Discussion started: 22 April 2022
© Author(s) 2022. CC BY 4.0 License.

Atmospheric Chemistry and Physics Discussions

experiment-3 compared to sensitivity experiment-1 concerning MARGA observations, none of the model experiments capture the diurnal cycle of NH_3. Higher levels of observed NH_3 during daytime and modeled NH_3 during night-time highlight the need to develop diurnal variability in NH_3 emissions over this region. The increased HCl emissions in sensitivity experiment-3 improved the linear correlation between modelled and measured NH_4^+ concentration (r = 0.76) compared with the sensitivity experiment-1 (r = 0.45). By contrast, the NH_x (Fig. 9c) concentration does not significantly change its correlation coefficient between MARGA and model with values of 0.69, 0.70, and 0.70 for the sensitivity experiments 1, 2, and 3, respectively. The NMB for NH_3 reduced from 138 % to 113 %, NMB for NH_4^+ systematically improved from -61 % to 3 %. In contrast, NMB for NH_x increased from 12 % to 39 % for the simulations demonstrated by sensitivity experiments 1 and 3, respectively, in the model. Table 2 summarizes the statistical indicators for the three sensitivity experiments. NH_4Cl formation in the sensitivity experiment-3 leads to a higher mass concentration of ammonium, which also increases NH_x mass concentration by 27 %. We find consistent high bias in all the simulations of NH_3, which is the highest during early morning and night time (Fig. S7 in the Supplement).

Figure S8 in the Supplement illustrates a time-series graph that compares daily mean ammonia (Fig. S8a), ammonium (Fig. S8b), and total ammonia concentration (Fig. S8c) for the three different sensitivity experiments. Table 3 shows the mean ± standard deviation of these variables. The results show that compared to experiment 1, NH_3 concentrations decreased by 4 % in the sensitivity experiment-2 and further decreased by 10 % in the sensitivity experiment-3. On the contrary, NH_4^+ concentration improves in sensitivity experiment-2 by 54 % and further increases by 150 % (sensitivity experiment-3). This decrease in NH_3 is associated with the gas-to-particle conversion of NH_3 to NH_4^+. Since NH_4^+ concentration seems to be very sensitive to the increase in HCl emissions in the sensitivity experiment-3 (150 % improvement in NH_4^+), total ammonia also increased by 8.68 % and 24 % in the sensitivity experiment-2 and 3 respectively compared to the sensitivity experiment-1.

3.6 Observed and modeled (sensitivity experiment-3) diurnal variation

Here, diurnal variation of monitored aerosols and gases were analysed to investigate the gas-to-particle conversion of NH_3 in the model. We analyzed the simulation results of the sensitivity experiment-3**.** The diurnal variations in aerosol species and gaseous precursors are controlled mainly by thermodynamic gas-to-particle partitioning, PBL mixing, emission and deposition processes, along with vertical and horizontal advection (Meng et al., 2018). Figure 10 presents the diurnal variation of NH_3, Cl^-, NO_3^-, SO_4^{2-}, NH_4^+, HCl, SO_2, HONO, and HNO_3 concentrations in MARGA (Fig. 10a) and model (Fig. 10b). In the measurements (Fig.10a), between 19:00 and 9:00 h, a decrease in NH_3 was accompanied by an increase in NH_4^+ (r = -0.38), which coincided with higher Cl^- (r = -0.45) concentrations, while an increase in NH_3 coincided well with decreased NH_4^+ and Cl^-. Correlation of Cl^- with NH_4^+ shows a strong positive relation of r = 0.98, pointing to the chloride being the dominant neutralizing agent for NH_4^+ at the observational site (Acharja et al., 2021). Also, day and night formation of HONO and HNO_3 showed significant inverse correlations with NH_3 concentrations of r = -0.55 and r = -0.45, respectively. Furthermore, HONO formation showed a strong positive correlation of r = 0.68 with NH_4^+ concentration and r = 0.69 with Cl^- concentration. Low night-time temperature acts as a driver for aerosol formation, and the presence of NH_3 in the IGP may play a crucial role in promoting the hydrolysis of NO_2 and other heterogeneous reactions, resulting in explosive HONO and aerosol formation (Ge et al., 2019). However, in detail, the role of NH_3 and HONO formation in accelerating the secondary aerosol formation via

https://doi.org/10.5194/acp-2022-237
Preprint. Discussion started: 22 April 2022
© Author(s) 2022. CC BY 4.0 License.

Atmospheric Chemistry and Physics Discussions

heterogeneous reaction pathway requires further study. Our observations indicate that HCl, along with HONO and HNO_3, might play a significant role in determining the chemistry of NH_3 and other aerosols, similar to other studies Acharja et al. (2021) and Fu et al. (2019).

However, after including HCl emissions from trash burning (Sharma et al., 2019) in the model (Fig. 10b), the diurnal variation in NH_3 is found to be controlled mainly by strong linear relation of r = 0.81 with Cl^-, r = 0.79 with SO_2 and NH_4^+, r = 0.48 with NO_3^- and inverse relation r = -0.96 with HCl concentration. It should be noted that other than trash burning, various industrial plants around Delhi contribute to HCl emissions but are not considered in this emission inventory (Jaiprakash et al., 2017). In the model, a high concentration of Cl^-, SO_2, and NO_3^- mainly controls the diurnal behavior of NH_3. Significant missing daytime HONO sources include heterogeneous ground conversion, heterogeneous aerosol formation, soil emissions, and photochemical production, which are entirely missing in the model studies (Lu et al., 2018). A few possibilities might contribute to the modeled discrepancies. First, there are uncertainties in the emission inventory of the bottom-up approach of NH_3, SO_2, and NO_X, since NH_3, SO_2, and NO_X concentrations are overestimated in the model. Also, accurate industrial sources of HCl emission need to be included in the future. Work aimed at improving NH_3 emissions by considering agricultural statistics on fertilizer use and animal number distribution is currently under development as part of the Global Challenges Research Fund (GCRF), South Asian Nitrogen Hub (SANH). Second, the low gas-to-aerosol partitioning of SO_2 to sulfate in the WRF-Chem model, along with the overestimation of nitrate, can result in the discrepancies of sulfate, SO_2, and nitrate concentration. Third, missing HONO formation and chemical reactions catalyzed by TMI or oxidation by NO_2 in the MOSAIC mechanism is usually responsible for ~ 49 % of the SO_2 oxidation in a fog/haze situation, and the rest via O_3 oxidation (51 %) pathway is low in the model. Correct gas-to-aerosol partitioning of HNO_3 in the model significantly diminishes daytime nitrate and sulfate formation, which also obstructs the heterogeneous reaction of SO_2 with NO_2 thus leading to a positive NH_3 bias during wintertime in Delhi.

4. Conclusions

Ground-based measurements of NH_3, trace gases, and water-soluble ions in $PM_{2.5}$ were made during the WIFEX campaign from 19 December 2017 to 21 January 2018 at Indira Gandhi International Airport (IGIA) in the Indo-Gangetic Plain (IGP), where a large amount of ammonia is emitted because of agricultural and other activities. The averaged NH_3 and NH_4^+ concentrations measured by the MARGA instrument for the entire period were 28.20 and 36.96 µg m^{-3} compared with 56.75 and 14.71 µg m^{-3} as estimated by the WRF-Chem model, respectively. The bivariate polar plot of the gas-to-particle conversion of ammonia (NH_4^+/NH_3) shows a sporadic high value towards the west, indicating the dominance of ammonium and chloride formation. The share of major components of gases and particulate matter ($PM_{2.5}$) based on µeq m^{-3} shows, on average, the anions in $PM_{2.5}$ are almost exactly neutralized by NH_4^+ (49.54 %), with Cl^- (29.69 %) as the major anion. Furthermore, the observations show NH_4^+/NH_3 being significantly correlated (r = 0.79) with aerosol chloride concentration, with a much lower correlation for other anions, suggesting that ammonium chloride formation is predominant at the observational site. Modeled values overestimated NH_3 (56.75 µg m^{-3}) and underestimated NH_4^+ (14.71 µg m^{-3}) concentration in the WRF-Chem model. To evaluate the performance efficiency of the model, we conducted three sensitivity experiments in the model, sensitivity experiment-1 (default set-up without HCl emissions),

https://doi.org/10.5194/acp-2022-237
Preprint. Discussion started: 22 April 2022
© Author(s) 2022. CC BY 4.0 License.

Atmospheric Chemistry and Physics Discussions

sensitivity experiment-2 with base case HCl emissions (3 × original HCl emissions of Sharma et al. (2019)), and the sensitivity experiment-3 (3 × the base case HCl emissions) from trash burning to study its effect on the gas-to-aerosol partitioning of NH_3. The sensitivity experiment-3 results in significant improvements in the simulation of NH_4^+ concentration (range up to 70 µg m^{-3}), Cl^- concentration (range up to 110 µg m^{-3}), and some improvement in NH_3 observed at IGIA, Delhi.

Furthermore, for the first time, this study reports observed and modeled HCl concentrations that were promoting gas-to-particle conversion of ammonia by enhancing chloride concentration, suggesting that significant emissions of HCl into an ammonia-rich atmosphere facilitate the gas-to-particle conversion of ammonia through NH_4Cl formation. Although improvement is seen and there is a decrease in NH_3 gas-phase concentration by 10 % in the sensitivity experiment-3, the model still shows a high bias for NH_3 concentration. This suggests that the emissions inventory overestimates emissions of NH_3, along with SO_2 and NO_x, and highlights an incorrect gas-partitioning of NH_3 in the model.

This analysis is the first in South Asia to use simultaneous measurements from MARGA of NH_3, HNO_3, HCl, and aerosols combined with a high-resolution model to understand the coupling between gas-particles governing ammonia concentration. Our observations indicate that excess NH_3 concentrations along with daytime and night-time HNO_3 and HONO variability may impact secondary aerosol formation. However, to understand atmospheric photochemistry and heterogeneous chemical processes, the study of HONO and HNO_3 production mechanisms are required in the future. The accuracy of the chemical transport model is also affected by underestimation of SO_4^{2-}, HONO, HNO_3, and HCl, along with overestimation of SO_2 and NO_3^- and their interaction which impacts the model performance for NH_3. Hence, in the future, it is necessary to evaluate the impact of the addition of correct industrial sources of HCl emission along with appropriate emissions of HONO, SO_2, NH_3, and NO_x and the addition of missing chemical reactions catalyzed by TMI, or oxidation by NO_2 in the MOSAIC mechanisms which may improve the model-measurement agreement of the gas phase ammonia.

The present study suggests that the bias in NH_3 could be reduced by using country-specific emission inventories of NH_3, which are currently under development as part of the Global Challenges Research Fund (GCRF), South Asian Nitrogen Hub (SANH). Also, there is potential to develop top-down constraints on NH_3 emissions by taking inference from the satellite, model, and ground-based observations. Further examination of the role of wintertime biomass burning on NH_4^+/NH_3 partitioning is also merited, as this may provide a context further promoting NH_4^+ formation. Therefore, further substantial addition of appropriate emissions of the trace gases along with advanced chemistry is suggested to address the challenges of simulating atmospheric ammonia over the IGP region. Finally, the study highlights the importance of including the treatment of HCl and its anthropogenic emissions in modeling activities aimed at quantifying the role of NH_3 as a contributor to particulate matter.

Data availability

The 0.1° × 0.1° emission grid maps can be downloaded from the EDGAR website on https://edgar.jrc.ec.europa.eu/htap_v2/index.php?SECURE=_123 per year per sector. Gridded emissions in t y^{-1} on a 0.1° × 0.1° for HCl emissions can be downloaded from Mendeley data: http://dx.doi.org/10.

https://doi.org/10.5194/acp-2022-237
Preprint. Discussion started: 22 April 2022
© Author(s) 2022. CC BY 4.0 License.

Atmospheric Chemistry and Physics Discussions

581 17632/546t9249bv.1. The model data is available at Aditya, Indian Institute of Tropical Meteorology
582 (IITM) super-computer and can be provided upon request to the corresponding author. The observational and
583 meteorological data of WiFEX are available by contacting the corresponding author.

584 **Author contributions**

585 SDG designed the research; PVP performed the WRF-Chem model simulations and led the analysis; PA and RK
586 contributed to data collection and its quality control and assurance; GG, RK, and PG helped with the model set-
587 up; PVP and SDG wrote the paper with contributions from all co-authors.

588 **Competing interests**

589 The authors declare that they have no conflict of interest.

590 **Acknowledgments**

591 We thank the Director, IITM, for his continuous support and encouragement. IITM is funded by the Ministry of
592 Earth Sciences (MoES), Government of India. We wish to thank the MoES for supporting the WiFEX
593 campaign. The lead author's fellowship was supported by the National Supercomputing Mission (NSM)
594 program grant at C-DAC, and Ph.D. fees are covered by the Natural Environment Research Council (NERC) of
595 UK Research and Innovation (UKRI)-Global Challenges Research Fund (GCRF), South Asian Nitrogen Hub
596 (SANH), and we are grateful to the Executive Director and the Director-General of C-DAC and the SANH
597 Director and Chair of the Executive Board. We acknowledge the availability of CPCB-NO_x, NO_2, and O_3 data
598 from the CPCB web portal (https://app.cpcbccr.com/ccr, last access: 1 December 2021). We wish to
599 acknowledge the National Center for Atmospheric Research is sponsored by the National Science Foundation.

600 **5. References**

601 Acharja, P., Ali, K., Trivedi, D. K., Safai, P. D., Ghude, S., Prabhakaran, T. and Rajeevan, M.: Characterization
602 of atmospheric trace gases and water soluble inorganic chemical ions of PM_1 and $PM_{2.5}$ at Indira Gandhi
603 International Airport, New Delhi during 2017–18 winter, Sci. Total Environ., 729, 138800,
604 doi:10.1016/j.scitotenv.2020.138800, 2020.
605 Acharja, P., Ali, K., Ghude, S. D., Sinha, V., Sinha, B., Kulkarni, R., Gultepe, I. and Nair, M.: Chemosphere
606 Enhanced secondary aerosol formation driven by excess ammonia during fog episodes, Chemosphere,
607 289(November 2021), 133155, doi:10.1016/j.chemosphere.2021.133155, 2021.
608 Ali, K., Acharja, P., Trivedi, D. K., Kulkarni, R., Pithani, P., Safai, P. D., Chate, D. M., Ghude, S., Jenamani, R.
609 K. and Rajeevan, M.: Characterization and source identification of $PM_{2.5}$ and its chemical and carbonaceous
610 constituents during Winter Fog Experiment 2015–16 at Indira Gandhi International Airport, Delhi, Sci. Total
611 Environ., 662, 687–696, doi:10.1016/j.scitotenv.2019.01.285, 2019.
612 Archer-Nicholls, S., Lowe, D., Utembe, S., Allan, J., Zaveri, R. A., Fast, J. D., Hodnebrog, Ø., van der Gon, H.

© Author(s) 2022. CC BY 4.0 License.

and McFiggans, G.: Gaseous chemistry and aerosol mechanism developments for version 3.5.1 of the online regional model, WRF-Chem, Geosci. Model Dev., 7(6), 2557–2579, doi:10.5194/gmd-7-2557-2014, 2014.

Balzarini, A., Pirovano, G., Honzak, L., Žabkar, R., Curci, G., Forkel, R., Hirtl, M., San José, R., Tuccella, P. and Grell, G. A.: WRF-Chem model sensitivity to chemical mechanisms choice in reconstructing aerosol optical properties, Atmos. Environ., 115, 604–619, doi:10.1016/j.atmosenv.2014.12.033, 2015.

Behera, S. N., Sharma, M., Aneja, V. P. and Balasubramanian, R.: Ammonia in the atmosphere: a review on emission sources, atmospheric chemistry and deposition on terrestrial bodies, Environ. Sci. Pollut. Res., 20(11), 8092–8131, doi:10.1007/s11356-013-2051-9, 2013.

Bucaram, C. J. and Bowman, F. M.: WRF-Chem Modeling of Summertime Air Pollution in the Northern Great Plains : Chemistry and Aerosol Mechanism Intercomparison, Atmosphere (Basel)., 12(1121), 23, 2021.

Carslaw, D. C. and Ropkins, K.: Openair - An r package for air quality data analysis, Environ. Model. Softw., 27–28(July 2019), 52–61, doi:10.1016/j.envsoft.2011.09.008, 2012.

Cash, J. M., Langford, B., Di Marco, C., Mullinger, N. J., Allan, J., Reyes-Villegas, E., Joshi, R., Heal, M. R., Acton, W. J. F., Hewitt, C. N., Misztal, P. K., Drysdale, W., Mandal, T. K., Shivani, Gadi, R., Gurjar, B. R. and Nemitz, E.: Seasonal analysis of submicron aerosol in Old Delhi using high-resolution aerosol mass spectrometry: chemical characterisation, source apportionment and new marker identification, Atmos. Chem. Phys., 21(13), 10133–10158, doi:10.5194/acp-21-10133-2021, 2021.

Chate, D., Ghude, S., Beig, G., Mahajan, A., Jena, C., Reka, S., Dahiya, A. and Kumar, N.: Deviations from the O_3–NO–NO_2 photo-stationary state in Delhi, India, Atmos. Environ., 96, 353–358, doi:10.1016/j.atmosenv.2014.07.054, 2014.

Chaudhary, P., Garg, S., George, T., Shabin, M., Saha, S., Subodh, S. and Sinha, B.: Underreporting and open burning – the two largest challenges for sustainable waste management in India, Resour. Conserv. Recycl., 175, 105865, doi:https://doi.org/10.1016/j.resconrec.2021.105865, 2021.

Clarisse, L., Clerbaux, C., Dentener, F., Hurtmans, D. and Coheur, P. F.: Global ammonia distribution derived from infrared satellite observations, Nat. Geosci., 2(7), 479–483, doi:10.1038/ngeo551, 2009.

Clarisse, L., Shephard, M. W., Dentener, F., Hurtmans, D., Cady-Pereira, K., Karagulian, F., Van Damme, M., Clerbaux, C. and Coheur, P. F.: Satellite monitoring of ammonia: A case study of the San Joaquin Valley, J. Geophys. Res. Atmos., 115(13), 1–15, doi:10.1029/2009JD013291, 2010.

CPCB: Annual Report 2014-15., 2014.

CPCB: Annual Report Annual Report., https://cpcb.nic.in/annual-report.php, 2020.

Van Damme, M., Clarisse, L., Whitburn, S., Hadji-Lazaro, J., Hurtmans, D., Clerbaux, C. and Coheur, P. F.: Industrial and agricultural ammonia point sources exposed, Nature, 564(7734), 99–103, doi:10.1038/s41586-018-0747-1, 2018.

Datta, A., Sharma, S. K., Harit, R. C., Kumar, V., Mandal, T. K. and Pathak, H.: Ammonia emission from subtropical crop land area in india, Asia-Pacific J. Atmos. Sci., 48(3), 275–281, doi:10.1007/s13143-012-0027-1, 2012.

Duan, X., Yan, Y., Peng, L., Xie, K., Hu, D., Li, R. and Wang, C.: Role of ammonia in secondary inorganic aerosols formation at an ammonia-rich city in winter in north China: A comparative study among industry, urban, and rural sites, Environ. Pollut., 291(May), 118151, doi:10.1016/j.envpol.2021.118151, 2021.

Ellis, R. A., Murphy, J. G., Markovic, M. Z., Vandenboer, T. C., Makar, P. A., Brook, J. and Mihele, C.: The

https://doi.org/10.5194/acp-2022-237
Preprint. Discussion started: 22 April 2022
© Author(s) 2022. CC BY 4.0 License.

653 influence of gas-particle partitioning and surface-atmosphere exchange on ammonia during BAQS-Met, Atmos.
654 Chem. Phys., 11(1), 133–145, doi:10.5194/acp-11-133-2011, 2011.
655 FINNv1.5: FINN Data, [online] Available from: http://bai.acom.ucar.edu/Data/fire/ (Accessed 15 April 2019),
656 n.d.
657 Fu, X., Wang, T., Zhang, L., Li, Q., Wang, Z., Xia, M., Yun, H., Wang, W., Yu, C., Yue, D., Zhou, Y., Zheng,
658 J. and Han, R.: The significant contribution of HONO to secondary pollutants during a severe winter pollution
659 event in southern China, Atmos. Chem. Phys., 19(1), 1–14, doi:10.5194/acp-19-1-2019, 2019.
660 Gani, S., Bhandari, S., Seraj, S., Wang, D. S., Patel, K., Soni, P., Arub, Z., Habib, G., Hildebrandt Ruiz, L. and
661 Apte, J. S.: Submicron aerosol composition in the world's most polluted megacity: the Delhi Aerosol Supersite
662 study, Atmos. Chem. Phys., 19(10), 6843–6859, doi:10.5194/acp-19-6843-2019, 2019.
663 Ge, S., Wang, G., Zhang, S., Li, D., Xie, Y., Wu, C., Yuan, Q., Chen, J. and Zhang, H.: Abundant NH3 in China
664 Enhances Atmospheric HONO Production by Promoting the Heterogeneous Reaction of SO_2 with NO_2,
665 Environ. Sci. Technol., 53(24), 14339–14347, doi:10.1021/acs.est.9b04196, 2019.
666 Georgiou, G. K., Christoudias, T., Proestos, Y., Kushta, J., Hadjinicolaou, P. and Lelieveld, J.: Air quality
667 modelling in the summer over the eastern Mediterranean using WRF-Chem: chemistry and aerosol mechanism
668 intercomparison, Atmos. Chem. Phys., 18(3), 1555–1571, doi:10.5194/acp-18-1555-2018, 2018.
669 Ghude, S., Kumar, R., Jena, C., Debnath, S., Kulkarni, R., Alessandrini, S., Biswas, M., Kulkrani, S., Pithani,
670 P., Kelkar, S., Sajjan, V., Chate, D., Soni, V., Singh, S., Nanjundiah, R. and Rajeevan, M.: Evaluation of $PM_{2.5}$
671 Forecast using Chemical Data Assimilation in the WRF-Chem Model: A Novel Initiative Under the Ministry of
672 Earth Sciences Air Quality Early Warning System for Delhi, India, Curr. Sci., 118,
673 doi:10.18520/cs/v118/i11/1803-1815, 2020.
674 Ghude, S. D.: Premature mortality in India due to $PM_{2.5}$ and ozone exposure, Geophys. Res. Lett., 1–8,
675 doi:10.1002/2013GL058740.Received, 2016.
676 Ghude, S. D., Fadnavis, S., Beig, G., Polade, S. D. and van der A, R. J.: Detection of surface emission hot spots,
677 trends, and seasonal cycle from satellite-retrieved NO_2 over India, J. Geophys. Res., 113(D20), D20305,
678 doi:10.1029/2007JD009615, 2008a.
679 Ghude, S. D., Jain, S. L., Arya, B. C., Beig, G., Ahammed, Y. N., Kumar, A. and Tyagi, B.: Ozone in ambient
680 air at a tropical megacity, Delhi: Characteristics, trends and cumulative ozone exposure indices, J. Atmos.
681 Chem., 60(3), 237–252, doi:10.1007/s10874-009-9119-4, 2008b.
682 Ghude, S. D., Van der A, R. J., Beig, G., Fadnavis, S. and Polade, S. D.: Satellite derived trends in NO_2 over the
683 major global hotspot regions during the past decade and their inter-comparison, Environ. Pollut., 157(6), 1873–
684 1878, doi:10.1016/j.envpol.2009.01.013, 2009.
685 Ghude, S. D., Lal, D. M., Beig, G., van der A, R. and Sable, D.: Rain-Induced Soil NO_x Emission From India
686 During the Onset of the Summer Monsoon: A Satellite Perspective, J. Geophys. Res., 115(D16), D16304,
687 doi:10.1029/2009JD013367, 2010.
688 Ghude, S. D., Pfister, G. G., Jena, C. K., Emmons, L. K., Kumar, R. and van der A, R. J.: Satellite constraints of
689 Nitrogen Oxide (NO_X) emissions from India based on OMI observations and WRF-Chem simulations, Geophys.
690 Res. Lett., 40(x), 423–428, doi:10.1029/2012gl053926, 2012.
691 Ghude, S. D., Kulkarni, S. H., Jena, C., Pfister, G. G., Beig, G., Fadnavis, S. and Van Der, R. J.: Application of
692 satellite observations for identifying regions of dominant sources of nitrogen oxides over the Indian

https://doi.org/10.5194/acp-2022-237
Preprint. Discussion started: 22 April 2022
© Author(s) 2022. CC BY 4.0 License.

693 subcontinent, J. Geophys. Res. Atmos., 118(2), 1075–1089, doi:10.1029/2012JD017811, 2013.
694 Ghude, S. D., Bhat, G. S., Prabhakaran, T., Jenamani, R. K., Chate, D. M., Safai, P. D., Karipot, A. K., Konwar,
695 M., Pithani, P., Sinha, V., Rao, P. S. P., Dixit, S. A., Tiwari, S., Todekar, K., Varpe, S., Srivastava, A. K., Bisht,
696 D. S., Murugavel, P., Ali, K., Mina, U., Dharua, M., Rao, Y. J., Padmakumari, B., Hazra, A., Nigam, N.,
697 Shende, U., Lal, D. M., Chandra, B. P., Mishra, A. K., Kumar, A., Hakkim, H., Pawar, H., Acharja, P.,
698 Kulkarni, R., Subharthi, C., Balaji, B., Varghese, M., Bera, S. and Rajeevan, M.: Winter fog experiment over the
699 Indo-Gangetic plains of India, Curr. Sci., 112(4), doi:10.18520/cs/v112/i04/767-784, 2017.
700 Ginoux, P., Chin, M., Tegen, I., Goddard, T. and In-, G.: Sources and distribution of dust aerosols simulated
701 with the GOCART model, J. Geophys. Res., 106, 20255–20273, doi:https://doi.org/10.1029/2000JD000053,
702 2001.
703 Gu, B., Zhang, L., Dingenen, R. Van, Vieno, M., Grinsven, H. J. Van, Zhang, X., Zhang, S., Chen, Y., Wang,
704 S., Ren, C., Rao, S., Holland, M., Winiwarter, W., Chen, D., Xu, J. and Sutton, M. A.: Abating ammonia is
705 more cost-effective than nitrogen oxides for mitigating $PM_{2.5}$ air pollution, Science (80-.)., 374(6568), 758–
706 762, doi:10.1126/science.abf8623, 2021.
707 Guenther, A., Karl, T., Harley, P., Wiedinmyer, C., Palmer, P. I. and Geron, C.: Estimates of global terrestrial
708 isoprene emissions using MEGAN (Model of Emissions of Gases and Aerosols from Nature), Atmos. Chem.
709 Phys., 6(11), 3181–3210, doi:10.5194/acp-6-3181-2006, 2006.
710 Gunthe, S. S., Liu, P., Panda, U., Raj, S. S., Sharma, A., Darbyshire, E., Reyes-Villegas, E., Allan, J., Chen, Y.,
711 Wang, X., Song, S., Pöhlker, M. L., Shi, L., Wang, Y., Kommula, S. M., Liu, T., Ravikrishna, R., McFiggans,
712 G., Mickley, L. J., Martin, S. T., Pöschl, U., Andreae, M. O. and Coe, H.: Enhanced aerosol particle growth
713 sustained by high continental chlorine emission in India, Nat. Geosci., 14(2), 77–84, doi:10.1038/s41561-020-
714 00677-x, 2021.
715 Harris, E., Sinha, B., Van Pinxteren, D., Tilgner, A., Fomba, K. W., Schneider, J., Roth, A., Gnauk, T.,
716 Fahlbusch, B., Mertes, S., Lee, T., Collett, J., Foley, S., Borrmann, S., Hoppe, P. and Herrmann, H.: Enhanced
717 role of transition metal Ion catalysis during In-Cloud oxidation of SO2 , Sci. (New York, N.Y.) , 340(6133),
718 727–730, doi:10.1126/science.1230911, 2013.
719 Hindustan Times: 66 dairies, six dyeing units shut down in east Delhi, Hindustan Times, 6th July,
720 https://www.hindustantimes.com/cities/others/66-dairies-six-dyeing-units-shut-down-in-east-delhi-
721 101625596156203.html, 2021.
722 Huang, X., Song, Y., Li, M., Li, J., Huo, Q., Cai, X., Zhu, T., Hu, M. and Zhang, H.: A high-resolution
723 ammonia emission inventory in China, Global Biogeochem. Cycles, 26(1), 1–14, doi:10.1029/2011GB004161,
724 2012.
725 Ianniello, A., Spataro, F., Esposito, G., Allegrini, I., Rantica, E., Ancora, M. P., Hu, M. and Zhu, T.: Occurrence
726 of gas phase ammonia in the area of Beijing (China), Atmos. Chem. Phys., 10(19), 9487–9503,
727 doi:10.5194/acp-10-9487-2010, 2010.
728 Ianniello, A., Spataro, F., Esposito, G., Allegrini, I., Hu, M. and Zhu, T.: Chemical characteristics of inorganic
729 ammonium salts in PM2.5 in the atmosphere of Beijing (China), Atmos. Chem. Phys., 11(21), 10803–10822,
730 doi:10.5194/acp-11-10803-2011, 2011.
731 Jaiprakash, Singhai, A., Habib, G., Raman, R. S. and Gupta, T.: Chemical characterization of PM1.0 aerosol in
732 Delhi and source apportionment using positive matrix factorization, Environ. Sci. Pollut. Res., 24(1), 445–462,

https://doi.org/10.5194/acp-2022-237
Preprint. Discussion started: 22 April 2022
© Author(s) 2022. CC BY 4.0 License.

733 doi:10.1007/s11356-016-7708-8, 2017.
734 Jena, C., Ghude, S. D., Kumar, R., Debnath, S., Govardhan, G., Soni, V. K., Kulkarni, S. H., Beig, G.,
735 Nanjundiah, R. S. and Rajeevan, M.: Performance of high resolution (400 m) PM2.5 forecast over Delhi, Sci.
736 Rep., 11(1), 1–9, doi:10.1038/s41598-021-83467-8, 2021.
737 Kulkarni, S. H., Ghude, S. D., Jena, C., Karumuri, R. K., Sinha, B., Sinha, V., Kumar, R., Soni, V. K. and
738 Khare, M.: How Much Does Large-Scale Crop Residue Burning Affect the Air Quality in Delhi?, Environ. Sci.
739 Technol., 54(8), 4790–4799, doi:10.1021/acs.est.0c00329, 2020.
740 Kumar, A., Hakkim, H., Ghude, S. D. and Sinha, V.: Probing wintertime air pollution sources in the Indo-
741 Gangetic Plain through 52 hydrocarbons measured rarely at Delhi & Mohali, Sci. Total Environ., 801, 149711,
742 doi:https://doi.org/10.1016/j.scitotenv.2021.149711, 2021.
743 Kumar, R., Ghude, S. D., Biswas, M., Jena, C., Alessandrini, S., Debnath, S., Kulkarni, S., Sperati, S., Soni, V.
744 K., Nanjundiah, R. S. and Rajeevan, M.: Enhancing Accuracy of Air Quality and Temperature Forecasts During
745 Paddy Crop Residue Burning Season in Delhi Via Chemical Data Assimilation, J. Geophys. Res. Atmos.,
746 125(17), 1–16, doi:10.1029/2020JD033019, 2020.
747 Kuttippurath, J., Singh, A., Dash, S. P., Mallick, N., Clerbaux, C., Van Damme, M., Clarisse, L., Coheur, P. F.,
748 Raj, S., Abbhishek, K. and Varikoden, H.: Record high levels of atmospheric ammonia over India: Spatial and
749 temporal analyses, Sci. Total Environ., 740, 139986, doi:10.1016/j.scitotenv.2020.139986, 2020.
750 Lan, Z., Lin, W., Pu, W. and Ma, Z.: Measurement report: Exploring NH_3 behavior in urban and suburban
751 Beijing: Comparison and implications, Atmos. Chem. Phys., 21(6), 4561–4573, doi:10.5194/acp-21-4561-2021,
752 2021.
753 Li, J., Zhang, Y. L., Cao, F., Zhang, W., Fan, M., Lee, X. and Michalski, G.: Stable Sulfur Isotopes Revealed a
754 Major Role of Transition-Metal Ion-Catalyzed SO2 Oxidation in Haze Episodes, Environ. Sci. Technol., 54(5),
755 2626–2634, doi:10.1021/acs.est.9b07150, 2020.
756 Lu, X., Wang, Y., Li, J., Shen, L. and Fung, J. C. H.: Evidence of heterogeneous HONO formation from
757 aerosols and the regional photochemical impact of this HONO source, Environ. Res. Lett., 13(11),
758 doi:10.1088/1748-9326/aae492, 2018.
759 Luhana, L., Middleton, D. R., Sokhi, R. S. and Great Britain. Environment Agency.: Processes and parameters
760 influencing the oxidation of SO2 and NOx in plumes., 2007.
761 Makkonen, U., Virkkula, A., Mäntykenttä, J., Hakola, H., Keronen, P., Vakkari, V. and Aalto, P. P.: Semi-
762 continuous gas and inorganic aerosol measurements at a Finnish urban site: comparisons with filters, nitrogen in
763 aerosol and gas phases, and aerosol acidity, Atmos. Chem. Phys., 12(12), 5617–5631, doi:10.5194/acp-12-5617-
764 2012, 2012.
765 Mandal, T. K., Saxena, M., Rohtash, Sharma, S. K., Gupta, N. C., Kumar, M. and Saraswati: Characteristics of
766 ambient ammonia over Delhi, India, Meteorol. Atmos. Phys., 124(1–2), 67–82, doi:10.1007/s00703-013-0299-
767 8, 2013.
768 Meng, Z., Xu, X., Lin, W., Ge, B., Xie, Y., Song, B., Jia, S., Zhang, R., Peng, W., Wang, Y., Cheng, H., Yang,
769 W. and Zhao, H.: Role of ambient ammonia in particulate ammonium formation at a rural site in the North
770 China Plain, Atmos. Chem. Phys., 18(1), 167–184, doi:10.5194/acp-18-167-2018, 2018.
771 Metzger, S., Mihalopoulos, N. and Lelieveld, J.: Importance of mineral cations and organics in gas-aerosol
772 partitioning of reactive nitrogen compounds: Case study based on MINOS results, Atmos. Chem. Phys., 6(9),

© Author(s) 2022. CC BY 4.0 License.

2549–2567, doi:10.5194/acp-6-2549-2006, 2006.

Móring, A., Hooda, S., Raghuram, N., Adhya, T. K., Ahmad, A., Bandyopadhyay, S. K., Barsby, T., Beig, G., Bentley, A. R., Bhatia, A., Dragosits, U., Drewer, J., Foulkes, J., Ghude, S. D., Gupta, R., Jain, N., Kumar, D., Kumar, R. M., Ladha, J. K., Mandal, P. K., Neeraja, C. N., Pandey, R., Pathak, H., Pawar, P., Pellny, T. K., Poole, P., Price, A., Rao, D. L. N., Reay, D. S., Singh, N. K., Sinha, S. K., Srivastava, R. K., Shewry, P., Smith, J., Steadman, C. E., Subrahmanyam, D., Surekha, K., Venkatesh, K., Varinderpal-Singh, Uwizeye, A., Vieno, M. and Sutton, M. A.: Nitrogen Challenges and Opportunities for Agricultural and Environmental Science in India, Front. Sustain. Food Syst., 5, 13, doi:10.3389/fsufs.2021.505347, 2021.

Nivdange, S., Jena, C. and Pawar, P.: Nationwide CoViD-19 lockdown impact on air quality in India, MAUSAM, 73(1), 115–128, doi:10.54302/mausam.v73i1.1475, 2022.

Norman, M., Spirig, C., Wolff, V., Trebs, I., Flechard, C., Wisthaler, A., Schnitzhofer, R., Hansel, A. and Neftel, A.: Intercomparison of ammonia measurement techniques at an intensively managed grassland site (Oensingen, Switzerland), Atmos. Chem. Phys., 9(8), 2635–2645, doi:10.5194/acp-9-2635-2009, 2009.

Pawar, P. V., Ghude, S. D., Jena, C., Móring, A., Sutton, M. A., Kulkarni, S., Lal, D. M., Surendran, D., Van Damme, M., Clarisse, L., Coheur, P.-F., Liu, X., Govardhan, G., Xu, W., Jiang, J. and Adhya, T. K.: Analysis of atmospheric ammonia over South and East Asia based on the MOZART-4 model and its comparison with satellite and surface observations, Atmos. Chem. Phys., 21(8), 6389–6409, doi:10.5194/acp-21-6389-2021, 2021.

Pinder, R. W., Adams, P. J. and Pandis, S. N.: Ammonia Emission Controls as a Cost-Effective Strategy for Reducing Atmospheric Particulate Matter in the Eastern United States, Environ. Sci. Technol., 41(2), 380–386, doi:10.1021/es060379a, 2007.

Pinder, R. W., Gilliland, A. B. and Dennis, R. L.: Environmental impact of atmospheric NH3 emissions under present and future conditions in the eastern United States, Geophys. Res. Lett., 35(12), doi:10.1029/2008GL033732, 2008.

Pollution, C. and Board, C.: Guidelines for Manual Sampling & Analyses., 2011.

Reyes-Villegas, E., Panda, U., Darbyshire, E., Cash, J. M., Joshi, R., Langford, B., Di Marco, C. F., Mullinger, N. J., Alam, M. S., Crilley, L. R., Rooney, D. J., Acton, W. J. F., Drysdale, W., Nemitz, E., Flynn, M., Voliotis, A., McFiggans, G., Coe, H., Lee, J., Hewitt, C. N., Heal, M. R., Gunthe, S. S., Mandal, T. K., Gurjar, B. R., Shivani, Gadi, R., Singh, S., Soni, V. and Allan, J. D.: PM$_{1}$ composition and source apportionment at two sites in Delhi, India, across multiple seasons, Atmos. Chem. Phys., 21(15), 11655–11667, doi:10.5194/acp-21-11655-2021, 2021.

Saraswati, George, M. P., Sharma, S. K., Mandal, T. K. and Kotnala, R. K.: Simultaneous Measurements of Ambient NH_3 and Its Relationship with Other Trace Gases, $PM_{2.5}$ and Meteorological Parameters over Delhi, India, Mapan - J. Metrol. Soc. India, 34(1), 55–69, doi:10.1007/s12647-018-0286-0, 2019.

Seinfeld, J. H. and Pandis, S. N.: Atmospheric chemistry and physics: from air pollution to climate change JohnWiley & Sons, Hoboken, New Jersey, 2016.

Sha, T., Ma, X., Jia, H., Tian, R., Chang, Y., Cao, F. and Zhang, Y.: Aerosol chemical component: Simulations with WRF-Chem and comparison with observations in Nanjing, Atmos. Environ., 218(June), 116982, doi:10.1016/j.atmosenv.2019.116982, 2019.

Sharma, C., Tiwari, M. K. and Pathak, H.: Estimates of emission and deposition of reactive nitrogenous species

https://doi.org/10.5194/acp-2022-237
Preprint. Discussion started: 22 April 2022
© Author(s) 2022. CC BY 4.0 License.

for India, Curr. Sci., 94(11), 1439–1446, 2008.

Sharma, G., Sinha, B., Pallavi, Hakkim, H., Chandra, B. P., Kumar, A. and Sinha, V.: Gridded Emissions of CO, NO_x, SO_2, CO_2, NH_3, HCl, CH_4, $PM_{2.5}$, PM_{10}, BC, and NMVOC from Open Municipal Waste Burning in India, Environ. Sci. Technol., 53(9), 4765–4774, doi:10.1021/acs.est.8b07076, 2019.

Sharma, S. K., Saxena, M., Saud, T., Korpole, S. and Mandal, T. K.: Measurement of NH_3, NO, NO_2 and related particulates at urban sites of indo gangetic plain (IGP) of India, J. Sci. Ind. Res. (India)., 71(5), 360–362, 2012.

Sharma, S. K., Harit, R. C., Kumar, V., Mandal, T. K. and Pathak, H.: Ammonia Emission from Rice-Wheat Cropping System in Subtropical Soil of India, Agric. Res., 3(2), 175–180, doi:10.1007/s40003-014-0107-9, 2014a.

Sharma, S. K., Kumar, M., Rohtash, Gupta, N. C., Saraswati, Saxena, M. and Mandal, T. K.: Characteristics of ambient ammonia over Delhi, India., 2014b.

Sharma, S. K., Kotnala, G. and Mandal, T. K.: Spatial Variability and Sources of Atmospheric Ammonia in India: A Review, Aerosol Sci. Eng., 4(1), doi:10.1007/s41810-019-00052-3, 2020.

Singh, G. K., Rajeev, P., Paul, D. and Gupta, T.: Chemical characterization and stable nitrogen isotope composition of nitrogenous component of ambient aerosols from Kanpur in the Indo-Gangetic Plains., Sci. Total Environ., 763, 143032, doi:10.1016/j.scitotenv.2020.143032, 2021.

Sutton, M. A. and Howard, C. M.: Ammonia maps make history, Nature, 564(7734), 49–50, 2018.

Sutton, M. A., Burkhardt, J. K., Guerin, D., Nemitz, E. and Fowler, D.: Development of resistance models to describe measurements of bi-directional ammonia surface-atmosphere exchange, Atmos. Environ., 32(3), 473–480, doi:10.1016/S1352-2310(97)00164-7, 1998.

Sutton, M. A., Asman, W. A. H., Ellerman, T., Acker, K., Aneja, V., Duyzer, J. H., Paramonov, S., Mitosinkova, M., Tang, Y. S., Achermann, B., Gauger, T., Bartnicki, J. and Neftel, A.: Establishing the link between ammonia emission control and measurements of reduced nitrogen concentrations and deposition . Establishing the link between ammonia emission control and measurements of reduced nitrogen concentrations and, Landscape, (September 2000), 57–84, 2001.

Sutton, M. A., Erisman, J. W., Dentener, F. and Möller, D.: Ammonia in the environment: From ancient times to the present, Environ. Pollut., 156(3), 583–604, doi:10.1016/j.envpol.2008.03.013, 2008.

Sutton, M. A., Reis, S. and Baker, S. M. H.: Atmospheric Ammonia: Detecting emission changes and environmental impacts., 2009.

Sutton, M. A., Reis, S., Riddick, S. N., Dragosits, U., Nemitz, E., Theobald, M. R., Tang, Y. S., Braban, C. F., Vieno, M., Dore, A. J., Mitchell, R. F., Wanless, S., Daunt, F., Fowler, D., Blackall, T. D., Milford, C., Flechard, C. R., Loubet, B., Massad, R., Cellier, P., Personne, E., Coheur, P. F., Clarisse, L., Van Damme, M., Ngadi, Y., Clerbaux, C., Skjøth, C. A., Geels, C., Hertel, O., Kruit, R. J. W., Pinder, R. W., Bash, J. O., Walker, J. T., Simpson, D., Horváth, L., Misselbrook, T. H., Bleeker, A., Dentener, F. and de Vries, W.: Towards a climate-dependent paradigm of ammonia emission and deposition, Philos. Trans. R. Soc. B Biol. Sci., 368(1621), 20130166–20130166, doi:10.1098/rstb.2013.0166, 2013.

Sutton, M. A., Drewer, J., Moring, A., Adhya, T. K., Ahmed, A., Bhatia, A., Brownlie, W., Dragosits, U., Ghude, S. D., Hillier, J., Hooda, S., Howard, C. M., Jain, N., Kumar, D., Kumar, R. M., Nayak, D. R., Neeraja, C. N., Prasanna, R., Price, A., Ramakrishnan, B., Reay, D. S., Singh, R., Skiba, U., Smith, J. U., Sohi, S., Subrahmanyan, D., Surekha, K., van Grinsven, H. J. M., Vieno, M., Voleti, S. R., Pathak, H. and Raghuram, N.:

https://doi.org/10.5194/acp-2022-237
Preprint. Discussion started: 22 April 2022
© Author(s) 2022. CC BY 4.0 License.

Atmospheric Chemistry and Physics Discussions

2 - The Indian Nitrogen Challenge in a Global Perspective, in The Indian Nitrogen Assessment, edited by Y. P. Abrol, T. K. Adhya, V. P. Aneja, N. Raghuram, H. Pathak, U. Kulshrestha, C. Sharma, and B. Singh, pp. 9–28, Elsevier., 2017a.

Sutton, M. A., J. Drewer, A. Moring, T.K Adhya, A. Ahmed and A. Bhatia: The Indian nitrogen assessment : sources of reactive nitrogen, environmental and climate effects, management options, and policies, in The Indian Nitrogen Assessment, edited by Y. P. Abrol, T. K. Adhya, V. P. Aneja, N. Raghuram, H. Pathak, U. Kulshrestha, C. Sharma, and B. Singh, pp. 9–25, Elsevier., 2017b.

Sutton, M. A., Van Dijk, N., Levy, P. E., Jones, M. R., Leith, I. D., Sheppard, L. J., Leeson, S., Sim Tang, Y., Stephens, A., Braban, C. F., Dragosits, U., Howard, C. M., Vieno, M., Fowler, D., Corbett, P., Naikoo, M. I., Munzi, S., Ellis, C. J., Chatterjee, S., Steadman, C. E., Móring, A. and Wolseley, P. A.: Alkaline air: changing perspectives on nitrogen and air pollution in an ammonia-rich world: Alkaline Air, Philos. Trans. R. Soc. A Math. Phys. Eng. Sci., 378(2183), doi:10.1098/rsta.2019.0315, 2020.

Technical specifications for CAAQM station: Technical Specifications For Continuous Ambient Air Quality Monitoring (CAAQM) Station (Real Time) Central Pollution Control Board East Arjun Nagar , Shahdara., 2019.

Thomas, R. M., Trebs, I., Otjes, R., Jongejan, P. A. C., Brink, H. ten, Phillips, G., Kortner, M., Meixner, F. X. and Nemitz, E.: An Automated Analyzer to Measure Surface-Atmosphere Exchange Fluxes of Water Soluble Inorganic Aerosol Compounds and Reactive Trace Gases, Environ. Sci. \& Technol., 43(5), 1412–1418, doi:10.1021/es8019403, 2009.

Trebs, I., Meixner, F. X., Slanina, J., Otjes, R., Jongejan, P. and Andreae, M. O.: Real-time measurements of ammonia, acidic trace gases and water-soluble inorganic aerosol species at a rural site in the Amazon Basin, Atmos. Chem. Phys., 4(4), 967–987, doi:10.5194/acp-4-967-2004, 2004.

Twigg, M. M., Di Marco, C. F., Leeson, S., van Dijk, N., Jones, M. R., Leith, I. D., Morrison, E., Coyle, M., Proost, R., Peeters, A. N. M., Lemon, E., Frelink, T., Braban, C. F., Nemitz, E. and Cape, J. N.: Water soluble aerosols and gases at a UK background site – Part 1: Controls of $PM_{2.5}$ and PM_{10} aerosol composition, Atmos. Chem. Phys., 15(14), 8131–8145, doi:10.5194/acp-15-8131-2015, 2015.

Wagh, S., Singh, P., Ghude, S. D., Safai, P., Prabhakaran, T. and Kumar, P. P.: Study of ice nucleating particles in fog-haze weather at New Delhi, India: A case of polluted environment, Atmos. Res., 259, 105693, doi:https://doi.org/10.1016/j.atmosres.2021.105693, 2021.

Wang, J., Li, J., Ye, J., Zhao, J., Wu, Y., Hu, J., Liu, D., Nie, D., Shen, F., Huang, X., Huang, D. D., Ji, D., Sun, X., Xu, W., Guo, J., Song, S., Qin, Y., Liu, P., Turner, J. R., Lee, H. C., Hwang, S., Liao, H., Martin, S. T., Zhang, Q., Chen, M., Sun, Y., Ge, X. and Jacob, D. J.: Fast sulfate formation from oxidation of SO2 by NO2 and HONO observed in Beijing haze, Nat. Commun., 11(1), 1–7, doi:10.1038/s41467-020-16683-x, 2020a.

Wang, S., Nan, J., Shi, C., Fu, Q., Gao, S., Wang, D., Cui, H., Saiz-Lopez, A. and Zhou, B.: Atmospheric ammonia and its impacts on regional air quality over the megacity of Shanghai, China, Sci. Rep., 5(October), 1–13, doi:10.1038/srep15842, 2015.

Wang, T., Song, Y., Xu, Z., Liu, M., Xu, T., Liao, W., Yin, L., Cai, X., Kang, L., Zhang, H. and Zhu, T.: Why is the Indo-Gangetic Plain the region with the largest NH_3 column in the globe during pre-monsoon and monsoon seasons?, Atmos. Chem. Phys., 20(14), 8727–8736, doi:10.5194/acp-20-8727-2020, 2020b.

Warner, J. X., Dickerson, R. R., Wei, Z., Strow, L. L., Wang, Y. and Liang, Q.: Increased atmospheric ammonia

https://doi.org/10.5194/acp-2022-237
Preprint. Discussion started: 22 April 2022
© Author(s) 2022. CC BY 4.0 License.

over the world's major agricultural areas detected from space, Geophys. Res. Lett., 44(6), 2875–2884, doi:10.1002/2016GL072305, 2017.

Xu, J., Chen, J., Huo, J., Lin, Y., Fu, Q., Guo, H. and Lee, S. H.: Importance of gas-particle partitioning of ammonia in haze formation in the rural agricultural environment, Atmos. Chem. Phys., 20(12), 7259–7269, doi:10.5194/acp-20-7259-2020, 2020.

Yang, J., Li, L., Wang, S., Li, H., Francisco, J. S., Zeng, X. C. and Gao, Y.: Unraveling a New Chemical Mechanism of Missing Sulfate Formation in Aerosol Haze: Gaseous NO_2 with Aqueous HSO_3^-/SO_3^{2-}, J. Am. Chem. Soc., 141(49), 19312–19320, doi:10.1021/jacs.9b08503, 2019.

Zaveri, R. A., Easter, R. C., Fast, J. D. and Peters, L. K.: Model for Simulating Aerosol Interactions and Chemistry (MOSAIC), J. Geophys. Res. Atmos., 113(13), 1–29, doi:10.1029/2007JD008782, 2008.

Zhang, L., Li, Q., Wang, T., Ahmadov, R., Zhang, Q., Li, M. and Lv, M.: Combined Impacts of Nitrous Acid and Nitryl Chloride on Lower Tropospheric Ozone: New Module Development in WRF-Chem and Application to China, Comb. Impacts Nitrous Acid Nitryl Chloride Low. Ozone New Modul. Dev. WRF-Chem and Application to China, 17(16), 1–31, doi:10.5194/acp-2017-389, 2017.

Zhang, X., Liu, J., Han, H., Zhang, Y., Jiang, Z., Wang, H., Meng, L., Li, Y. C. and Liu, Y.: Satellite-Observed Variations and Trends in Carbon Monoxide over Asia and Their Sensitivities to Biomass Burning, Remote Sens., 12(5), 830, doi:10.3390/rs12050830, 2020.

https://doi.org/10.5194/acp-2022-237
Preprint. Discussion started: 22 April 2022
© Author(s) 2022. CC BY 4.0 License.

Atmospheric Chemistry and Physics Discussions

FIGURE CAPTIONS

Figure 1. (a) Observed average diurnal variation in NH_3 and NH_4^+ with its (b) meteorological parameters during the sampling period (right).

Figure 2. (a) Wind rose diagram from the observational site, bivariate plots of (b) NH_3 concentration (c) Ammonium concentration (d) HCl concentration (e) Chloride concentration and (f) Partitioning ratio of NH_4^+/NH_x in relation to wind speed (m s^{-1}) and direction.

Figure 3. (a) Comparison of observed and simulated diurnal variation in NH_3 and NH_4^+ with its (b) meteorological parameters during the sampling period.

Figure 4. (a) Temporal variation in the daily mean NH_3 concentration, (b) NH_4^+ concentration, and (c) NH_x concentration for MARGA measurements (black line) and model (Redline).

Figure 5. Share of major components of gases and particulate matter ($PM_{2.5}$) based on the mean concentrations during WiFEX (share according to μeq m^{-3}).

Figure 6. Neutralizing effect between Cl^-, NO_3^- and SO_4^{2-} as the anions and aerosol neutralization ratio (ANR).

Figure 7. Relationship between observed NH_4^+/NH_x with (a) NH_4^+ and (b) Chloride concentration and Relationship between modeled NH_4^+/NH_x with (c) NH_4^+ and (d) Sulfate concentration at the IGIA site during the study period (red line denotes regression line).

Figure 8. Box-Whiskers plot for secondary inorganic aerosols, trace gases, and meteorological parameters from the observations and simulated by the model for the three different sensitivity experiments at Delhi.

Figure 9. Diurnal variation in the mean (a) NH_3 concentration (b) NH_4^+ concentration and (c) NH_x concentration for MARGA measurements (black), sensitivity experiment-1 (red dotted), sensitivity experiment-2 (red dash) and sensitivity experiment-3 (red solid).

Figure 10. Average diurnal cycles of ammonia with Cl^-, NO_3^-, SO_4^{2-}, NH_4^+, HCl, SO_2, HONO, and HNO_3 of (a) measured (MARGA) and (b) modeled (sensitivity experiment-3).

https://doi.org/10.5194/acp-2022-237
Preprint. Discussion started: 22 April 2022
© Author(s) 2022. CC BY 4.0 License.

Atmospheric Chemistry and Physics Discussions

973 **TABLES**

974 **Table 1. Performance of statistics of Correlation coefficient (*r*) of NH_4^+/NH_x with all other gases and**
975 **aerosols**
976

Gases and Aerosols	MARGA Correlation coefficient (*r*) with NH_4^+/NH_x ratio	Model Correlation coefficient (*r*) with NH_4^+/NH_x ratio
Ammonia (NH_3)	-0.57	-0.58
Sulfur dioxide (SO_2)	0.46	-0.30
Hydrogen chloride (HCl)	0.14	-
Nitrous acid (HONO)	-0.24	-0.23
Nitric acid (HNO_3)	0.33	0.46
Ammonium (NH_4^+)	0.70	0.67
Chloride (Cl^-)	0.79	-
Sulfate (SO_4^-)	0.09	0.77
Nitrate (NO_3^-)	0.13	0.57

977
978 **Table 2. Model performance statistics for NH_3, NH_4^+ and NH_x concentration at IGIA, Delhi from WRF-**
979 **Chem simulations and the MARGA**
980

Species	Sensitivity experiment-1		Sensitivity experiment-2		Sensitivity experiment-3	
	Correlation coefficient (*r*)	Normalised Mean Bias (NMB)	Correlation coefficient (*r*)	Normalised Mean Bias (NMB)	Correlation coefficient (*r*)	Normalised Mean Bias (NMB)
NH_3	-0.58	1.38	-0.60	1.29	-0.65	1.13
NH_4^+	0.45	-0.61	0.75	-0.40	0.76	-0.03
NH_x	0.69	0.12	0.70	0.22	0.70	0.39

981
982
983
984
985
986
987
988
989
990

https://doi.org/10.5194/acp-2022-237
Preprint. Discussion started: 22 April 2022
© Author(s) 2022. CC BY 4.0 License.

Atmospheric Chemistry and Physics Discussions

Table 3. Summary of ammonia, ammonium, and total ammonia concentration (daily mean ± standard deviation) in MARGA, sensitivity experiment-1, sensitivity experiment-2, and sensitivity experiment-3

Species	MARGA	Sensitivity experiment-1	Sensitivity experiment-2	Sensitivity experiment-3
NH_3 concentration (μg m^{-3})	20 ± 8.52	50.19 ± 11.79	48.18 ± 11.31	44.94 ± 10.80
NH_4^+ concentration (μg m^{-3})	35.94 ± 17.73	13.89 ± 3.04	21.44 ± 6.65	34.58 ± 15.21
NH_x concentration (μg m^{-3})	56.69 ± 17.15	164.08 ± 13.29	69.63 ± 16.66	79.52 ± 23.70

https://doi.org/10.5194/acp-2022-237
Preprint. Discussion started: 22 April 2022
© Author(s) 2022. CC BY 4.0 License.

Atmospheric Chemistry and Physics Discussions

1022 **Figure 1**

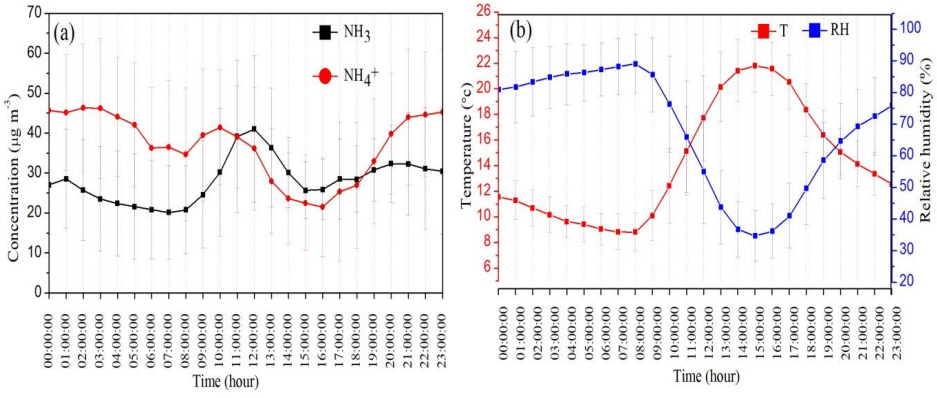

1023

1024 **Figure 2**

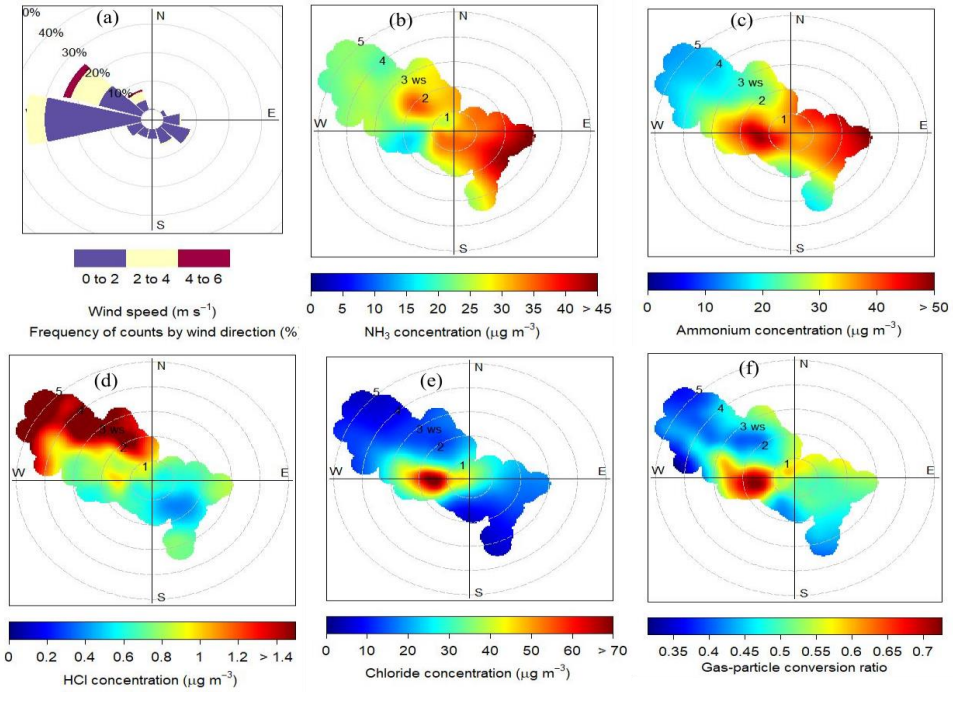

1025
1026
1027
1028
1029
1030

https://doi.org/10.5194/acp-2022-237
Preprint. Discussion started: 22 April 2022
© Author(s) 2022. CC BY 4.0 License.

Atmospheric Chemistry and Physics Discussions

1031 **Figure 3**

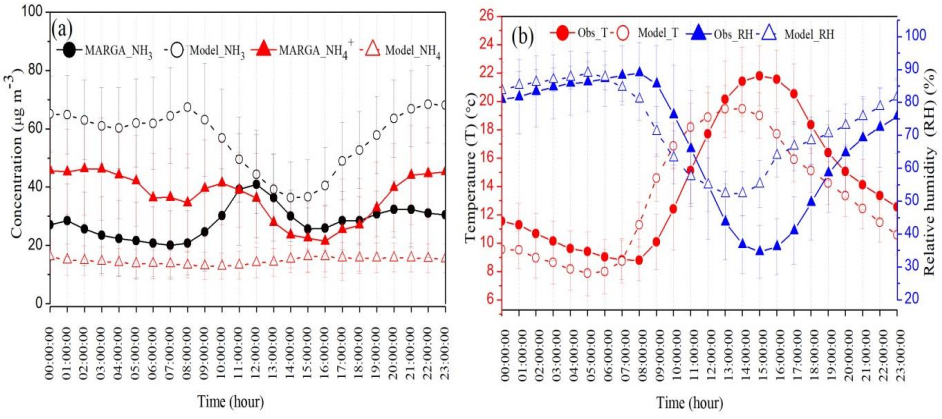

1032

1033 **Figure 4**

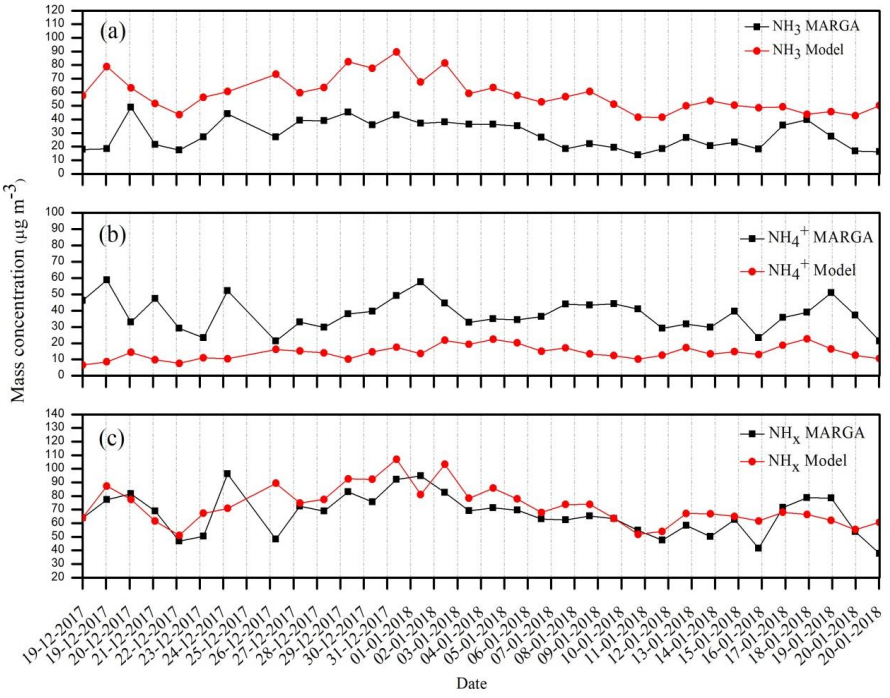

1034

1035

1036

1037

1038

https://doi.org/10.5194/acp-2022-237
Preprint. Discussion started: 22 April 2022
© Author(s) 2022. CC BY 4.0 License.

Atmospheric Chemistry and Physics Discussions

1039 **Figure 5**

1040

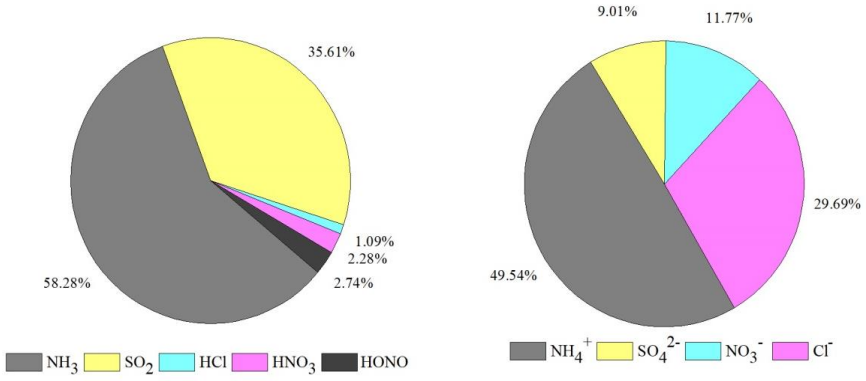

1041
1042

1043 **Figure 6**

1044

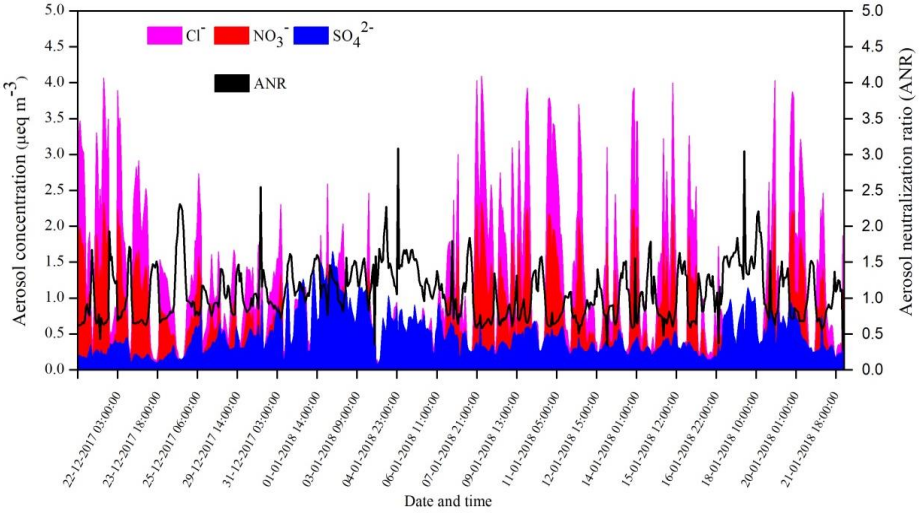

1045
1046
1047
1048
1049
1050
1051

https://doi.org/10.5194/acp-2022-237
Preprint. Discussion started: 22 April 2022
© Author(s) 2022. CC BY 4.0 License.

Atmospheric Chemistry and Physics Discussions

Figure 7

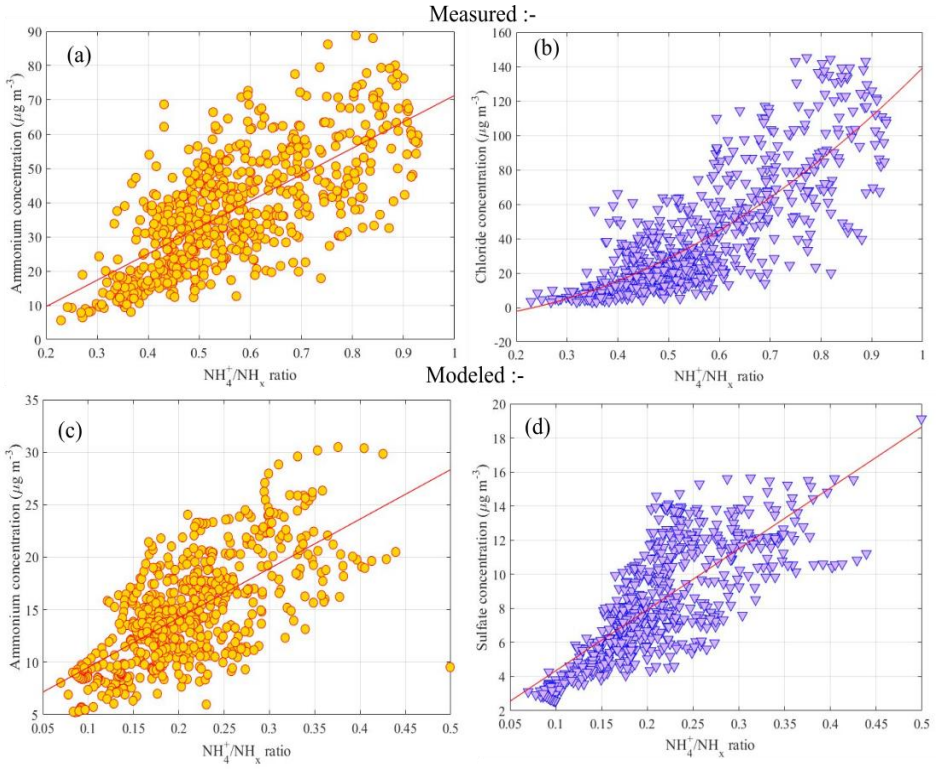

https://doi.org/10.5194/acp-2022-237
Preprint. Discussion started: 22 April 2022
© Author(s) 2022. CC BY 4.0 License.

Atmospheric Chemistry and Physics Discussions

1071 **Figure 8**

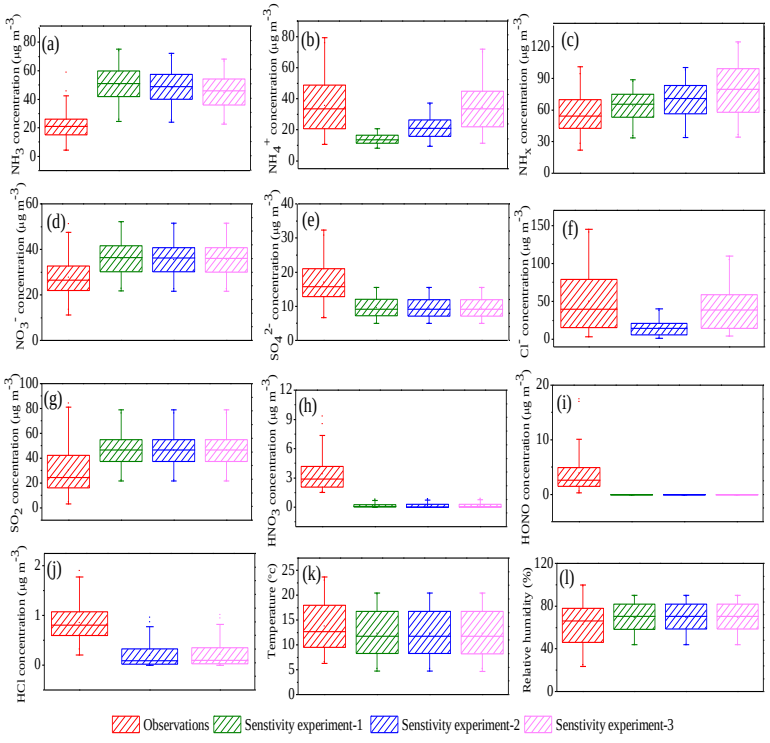

1072
1073
1074
1075
1076
1077
1078
1079
1080
1081
1082
1083
1084
1085
1086
1087
1088

https://doi.org/10.5194/acp-2022-237
Preprint. Discussion started: 22 April 2022
© Author(s) 2022. CC BY 4.0 License.

Atmospheric Chemistry and Physics Discussions

1089 **Figure 9**

1090

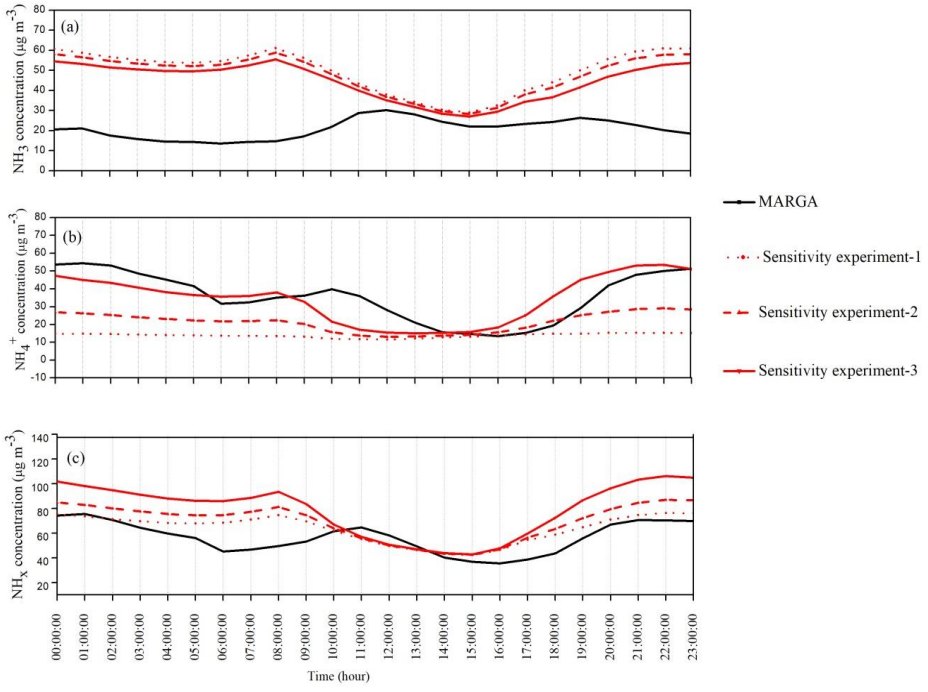

1091
1092
1093
1094
1095
1096
1097
1098
1099
1100
1101
1102
1103
1104
1105
1106
1107
1108
1109
1110

https://doi.org/10.5194/acp-2022-237
Preprint. Discussion started: 22 April 2022
© Author(s) 2022. CC BY 4.0 License.

Atmospheric Chemistry and Physics Discussions

1111 **Figure 10**

1112

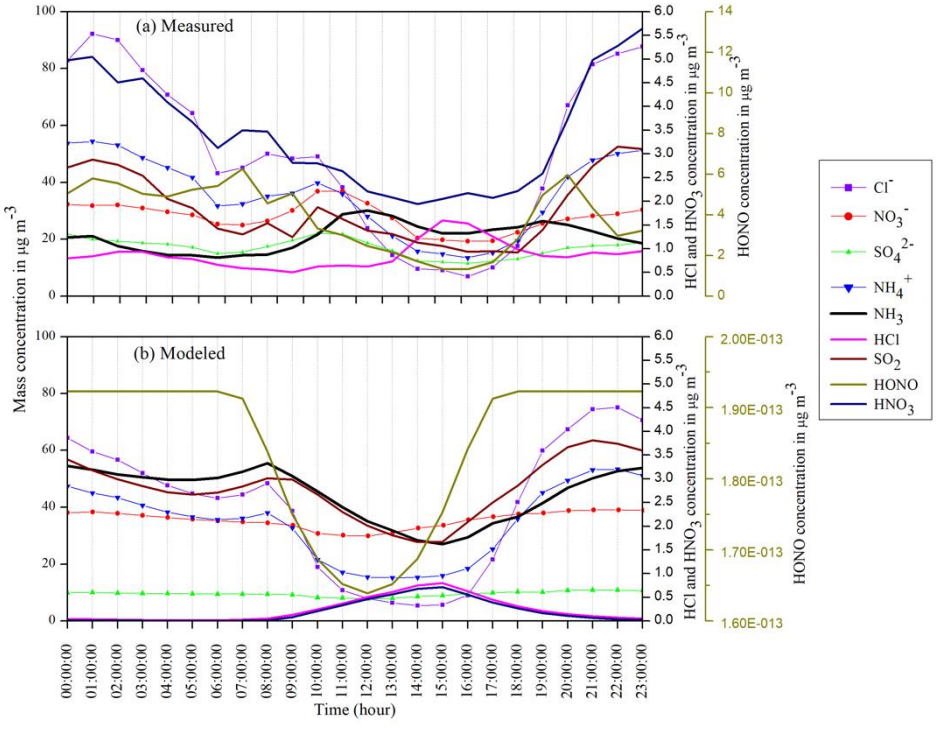

1113
1114
1115
1116
1117
1118
1119
1120
1121
1122
1123
1124
1125
1126
1127
1128
1129
1130
1131